Physics – Uspekhi **43** (5) 433 – 452 (2000)

REVIEWS OF TOPICAL PROBLEMS PACS numbers: 29.20.Dh, 29.27.Bd

Electron cooling: 35 years of development

V V Parkhomchuk, A N Skrinskiĭ¶

DOI: 10.1070/PU2000v043n05ABEH000741

Contents

Abstract. The electron cooling technique for shrinking ion beams of extremely high phase-space density was proposed and first tested at the Nuclear Physics Institute of the Siberian Branch of the Russian Academy of Sciences. The present review traces the history of the development of the idea from its first emergence in 1965 and the discussion originated in G I Budker's talk at the symposium on electron – positron rings in Sacle in September 1966 — through 35 years of research — down to the present time, with numerous applications in many acceleration centers around the world.

1. Origin of the idea and the first implementations of the method

1.1 Origin of the idea

In the 50s, studies of elementary particle structure that made use of collisions of accelerated particles with target nuclei encountered difficulties in achieving high energies in such interactions. The useful interaction energy in these collisions was an insignificant fraction of the primary particle energy and was mainly spent on the joint motion of the reaction products. A shift to experiments with two colliding beams of particles travelling counter to each other was the natural way out of the situation. In this case all the energy of the initial motion could be transformed into the energy of newly produced particles with large masses. Carrying out such experiments, however, required substantial improvements in the quality of beams in the accelerator.

The event rate $\mathrm{d}N/\mathrm{d}t$ of reactions with cross section σ depends on the luminosity of the facility, determined by the relation

$$L = \frac{\mathrm{d}N}{\mathrm{d}t}\,\frac{1}{\sigma} = f_\mathrm{b}\,\frac{N^2}{S} \sim I\,\frac{N}{S}\,, \qquad (1)$$

where N is the number of particles in the bunch, f_b is the collision frequency of bunches, S is the effective cross section of the particle bunches, and $I = Nf_\mathrm{b}e$ is the beam current. It can be seen that to enhance the luminosity it is necessary to increase both the current in the colliding beams and the particle density in the bunches.

The total, so-called six-dimensional, phase density of the beam, obtained from the source, cannot be increased by external fields independent of the particle motion (the Liouville theorem! [1]). The presence of dissipative forces causing the particles to lose energy makes possible the compression of the phase-space volume occupied by the beam. Projection of the beam's phase portrait onto the concrete 'coordinate – velocity' plane determines the emittance of the beam in this coordinate. Direct particle production at a new point of phase space due to a change in the

¶ The author is also known by the name A N Skrinsky. The name used here is a transliteration under the BSI/ANSI scheme adopted by this journal.

V V Parkhomchuk Nuclear Physics Institute, Siberian Branch of the Russian Academy of Sciences
prosp. ak. Lavrent'eva 11, 630090 Novosibirsk, Russian Federation
Tel. (7-3832) 39-44 61. Fax (7-3832) 34-21 63
E-mail: parkhomchuk@inp.nsk.su
A N Skrinskiĭ Russian Academy of Sciences, Nuclear Physics Division
Leninskiĭ prosp. 32a, 117993 Moscow, Russian Federation
Tel. (7-095) 938-07 53. Fax (7-095) 938-54 24
E-mail: skrinsky@inp.nsk.su

Received 13 February 2000
Uspekhi Fizicheskikh Nauk **170** (5) 473 – 493 (2000)
Translated by G Pontecorvo; edited by A Radzig

charge state while traversing the target resulting from charge exchange injection or from decays also serves as an example of violation of the Liouville theorem.

In the case of electrons and positrons it is relatively easy to organize conditions in which energy losses due to synchrotron radiation are sufficient for accumulating large currents in bunches with small emittances. Precisely this circumstance provided for the successful realization of colliding electron – positron beams. In the case of protons, manifestations of synchrotron radiation only appear at energies of many TeV, i.e. at energies that in the middle of the 60s seemed to be in the realm of unbridled fantasy.

Ionization losses occurring during the motion of particles in matter seemed the most natural candidate for dissipative forces. However, nuclear interaction with matter does not allow it to be used for strongly interacting particles, so ionization cooling will only become interesting, and even critically important, for huge muon colliders in the future [12].

The enhancement of the Coulomb interaction between particles at small relative velocities gave G I Budker [2] the idea to cool a proton beam with the aid of an electron beam moving with the same average velocity as the protons. When cooling is performed using such a beam, the temperatures determined by the respective electron and proton velocities V_e and V (in the co-moving frame of reference) level out: $mV_e^2/2 = MV^2/2$. As a result, the angular spread θ in the proton beam becomes significantly smaller than the angular spread θ_e in the electron beam:

$$\theta = \sqrt{\frac{m}{M}}\,\theta_e\,. \tag{2}$$

The first theoretical studies of cooling conditions [3] revealed that achieving a low electron temperature is a major problem for the successful realization of beam cooling.

Although the idea of the electron cooling of heavy particle beams was published and reported at several accelerator conferences, no one undertook any attempts to implement it before the first successful experiments were performed at the Nuclear Physics Institute of the RAS Siberian Branch.

1.2 NAP-M: the first electron cooling facility

In the conditions of an intense electron beam and, consequently, of a strong space charge, the task of focusing and joining beams determined whether electron cooling was to be successful or not.

Already the first proposal [2] quoted a 1-A current for the electron beam at an energy of 500 keV, which corresponded to a beam power of 0.5 MW. It was clear that, upon passing the cooling region once, the electron beam had to be recuperated and decelerated to the lowest possible level, and the electron energy returned to the source. In 1967 – 1970, a prototype electron cooler with a longitudinal magnetic field for compensating the defocusing effect of the electron beam space charge was under development [4, 5].

Experiments in recuperation of the electron beam permitted the creation of the NAP-M storage ring with electron cooling to be initiated in 1972. The name of the NAP-M facility (the Russian abbreviation for Accumulator of Anti-Protons — Model) reflected the goal of this facility: the storage of antiproton beams. The storage ring was to be created with a perimeter of 47.2 m; an electron cooler with an electron beam of effective length of about 1 m was installed in one of the straight sections.

In 1974, the cooling of a 65-MeV proton beam was successfully demonstrated. This took several seconds [6]. This time was close to the expected cooling times in accordance with the then existing estimates based on plasma approximations. The experiments, which were on the whole successful, revealed certain problems with the facility: the distributed vacuum pumps did not perform well in the cooling zone, questions arose relating to the stability of the accelerating voltages and to the beam diagnostics.

The experimental demonstration of electron cooling at the NAP-M facility gave rise to interest in this setup, and several delegations from the accelerator centers of CERN (Switzerland), FNAL (USA), GSI (Germany) visited the Nuclear Physics Institute of the RAS Siberian Branch in Novosibirsk to see for themselves the reality of electron cooling. After that, similar devices were constructed in many world laboratories for the development and practical use of the electron cooling technique.

1.3 The discovery of fast electron cooling

The conditions for accurate measurements improved significantly after the reconstruction of certain elements of the NAP-M storage ring and of the electron setup EPOKhA (the Russian abbreviation for Electron Beam for Cooling Antiprotons). Measurements of the dependence of the longitudinal drag friction force on the velocity difference between the electron and proton beams revealed that the drag force increases as the relative velocity between the beams decreases down to the smallest values, and then it changes sign, when the relative velocity reverses sign, as shown in Fig. 1.

The velocity distribution of electrons in the co-moving frame of reference was expected, from the first theoretical estimates, to be approximately spherically symmetric and to correspond to a cathode temperature of 0.2 eV and, thus, being close to the thermal electron velocity $V_e = \sqrt{kT/m} \approx 2 \times 10^7$ cm/s. Given the total velocity of motion of beam particles in the storage ring $V_0 = 10^{10}$ cm/s, one could assume that, starting from the relative velocity

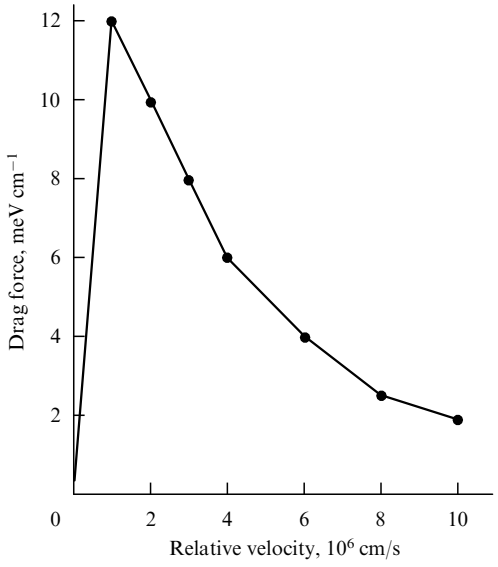

Figure 1. Measurements of the longitudinal drag force at NAP-M versus the relative velocity of electrons and protons. The proton beam energy was $E = 65$ MeV, the electron current $I_e = 0.3$ A, the density of the electron beam $n_e = 2.3 \times 10^8$ cm^{-3}.

$\Delta V = V - V_0 = 2 \times 10^7$ cm/s, the drag force would decrease as the proton velocity approached the equilibrium velocity V_0 but, as one can see from Fig. 1, the drag force actually increased at significantly smaller relative velocities ($\Delta V = 10^6$ cm/s $\ll V_e$).

The result obtained indicated that after acceleration in the electron gun, the spread of longitudinal velocities in the electron beam was significantly lower than the transverse velocity spread. In other words, the velocity distribution of electrons was strongly flattened in the longitudinal direction [7]. This is essentially a simple consequence of the Liouville theorem: the momentum spread decreases as the beam is expanded longitudinally during acceleration. The energy spread of electrons at the cathode amounts to kT, but after potential acceleration, which conserves the sum of potential and kinetic energies in the laboratory reference system ($\Delta E = p_0 \Delta V = kT$), the energy of longitudinal electron motion in the co-moving frame of reference becomes extremely insignificant:

$$kT_{\|} = kT \frac{kT}{\gamma^2 \beta^2 mc^2} , \tag{3}$$

where $\beta = V_0/c$, and $\gamma = (1 - \beta^2)^{-1/2}$. For the conditions of NAP-M one finds $kT = 0.2$ eV, $\gamma^2\beta^2 mc^2 = 10^5$ eV (the electron energy is 50 keV), which results in a 2×10^6-fold reduction in the longitudinal temperature. In these circumstances the longitudinal temperature is no longer determined by the initial electron spread, but by the mutual repulsion of electrons within the cooling zone.

The following fact was surprizing: the small longitudinal electron spread is conserved within the cooling zone and it drastically alters the kinetics of electron cooling, strongly enhancing the cooling rate. It was almost immediately understood that by 'magnetizing' the transverse electron motion, the magnetic field reduces the effective temperature of the electron beam by many orders of magnitude as compared to the cathode temperature [7–9]. The phenomenon of fast electron cooling that was discovered in this way, fundamentally altered the capabilities of the method and made it possible to obtain ion beams with energies of hundreds of MeV/nucleon and a temperature spread of fractions of a kelvin in the co-moving frame of reference [10–12].

2. Fundamentals of electron cooling theory

2.1 The drag force in the absence of a magnetic field

The field of a heavy particle moving in an electron gas causes perturbation of the electrons by imparting part of its energy of motion to them. In flying past an electron at an impact parameter ρ with a velocity V, a particle with charge Ze transfers to the electron a momentum

$$\Delta p_{\perp} = \frac{2Ze^2}{\rho V} . \tag{4}$$

The interaction process at small distances is accompanied by an enhancement of the momentum transfer in close collisions, and in the region of minimal impact parameters

$$\rho_{\min} = \frac{Zr_e}{(V/c)^2} , \tag{5}$$

where r_e is the classical electron radius, the transferred momentum reaches its largest possible value $2mV$. In the case of smaller impact parameters, it is no longer possible to restrict oneself to the Born approximation, in which the electron is assumed to be at rest in the collision process.

In the region of large impact parameters, restrictions arise when the mutual influence of electrons in the intense electron beam is taken into account. If the time $\tau_i = \rho/V$ it takes the particle to pass by the electron approaches the time for which Debye shielding is established owing to plasma oscillations with a frequency $\omega_e = c\sqrt{4\pi n_e r_e}$, the interaction efficiency is reduced for

$$\rho > \rho_{\max} = \frac{V}{\omega_e} . \tag{6}$$

In the region of intermediate impact parameters ρ, it is easy to calculate the mean energy loss of a particle moving in an electron gas:

$$\frac{dE}{dt} = -\int_{\rho_{\min}}^{\rho_{\max}} \frac{\Delta p_{\perp}^2}{2m} n_e V \cdot 2\pi\rho \, d\rho = \frac{4\pi Z^2 e^4 n_e L_c}{mV} , \tag{7}$$

where the Coulomb logarithm

$$L_c = \ln \frac{\rho_{\max}}{\rho_{\min}} , \tag{8}$$

and the drag force ($\mathbf{F} \cdot \mathbf{V} = dE/dt$):

$$\mathbf{F} = -\frac{4\pi Z^2 e^4 n_e L_c}{mV^3} \mathbf{V} . \tag{9}$$

If it is necessary to take into account the proper thermal motion of the electrons in the beam, the drag force is averaged over the velocity distribution $f_e(\mathbf{V}_e)$. Such integrals are most readily computed applying the Coulomb analogy of force in velocity space (neglecting the change in the Coulomb logarithm L_c).

Assume the velocity distribution of the electrons to have the shape of a flat disk with a transverse radius $V_{e\perp}$ and longitudinal width $\pm V_{e\|}$, and consider $V_{e\|} \ll V_{e\perp}$. In this case, the longitudinal drag force takes the form

$$F_{\|} = -\frac{8\pi Z^2 e^4 n_e L_c}{mV_{e\perp}^2} \begin{cases} \dfrac{V_{\|}}{V_{e\|}} , & |V_{\|}| < V_{e\|} , \\ \dfrac{V_{\|}}{|V_{\|}|} - \dfrac{V_{\|}}{\sqrt{V_{\|}^2 + V_{e\perp}^2}} , & |V_{\|}| > V_{e\|} . \end{cases} \tag{10}$$

At velocities $V_{\|} < V_{e\|}$ within the electron distribution, the longitudinal drag force increases rapidly; in the region $V_{e\|} < V_{\|} < V_{e\perp}$ it falls weakly, and, when $V_{\|} > V_{e\perp}$, it decreases rapidly (in proportion to V^{-2}), as shown in Fig. 2. The drag force is seen to fall rapidly (in proportion to $V_{e\perp}^{-3}$) at a high electron beam temperature, and the possibility of attaining high decrements is limited by the fast motion of electrons (with a velocity $V_{e\perp} \gg V$).

2.2 The drag force in a strong magnetic field

The longitudinal magnetic field B accompanying the electron beam in the cooling zone alters the drag force significantly. The reason for such a phenomenon is that owing to the thermal motion, the electron radius of Larmor gyration $\rho_L = mV_{e\perp}c/eB$ may be significantly smaller than the maximum impact parameter: $\rho_L \ll \rho_{\max}$. The transverse thermal

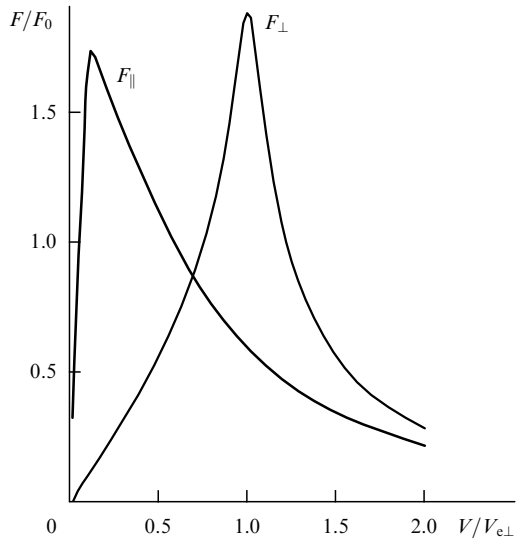

Figure 2. Variation of the longitudinal and transverse drag force components for a flattened electron velocity distribution at $V_{e\parallel} = 0.1V_{e\perp}$. The drag force is measured in units of $F_0 = 8\pi Z^2 e^4 n_e L_c / mV_{e\perp}^2$, and the velocity in units of $V_{e\perp}$.

motion of electrons in the 'magnetized' zone of impact parameters exerts no influence on the interaction kinetics of protons and electrons, while the contribution of electrons from this region of impact parameters to the drag force increases strongly and becomes predominant.

Figure 3 shows the change in momentum of a proton passing by an electron at a distance ρ in the case of magnetic fields B equal to 0, 100, and 1000 G. Multiplication of the change in proton momentum by ρ^2 permits a more correct comparison of the contributions of different impact parameters to the total drag force with due regard for the change in the number of electrons present in the volume element $n_e V\tau \cdot 2\pi\rho\, d\rho$:

$$F = \int_{-\infty}^{\infty} (\Delta p \cdot \rho^2)\, n_e V \cdot 2\pi \frac{d\rho}{\rho}\,. \tag{11}$$

The constancy of the product $\Delta p \cdot \rho^2$ within the range of impact parameters (ρ_1, ρ_2) indicates that the contribution of this region of impact parameters to the drag force is $\Delta p \cdot \rho^2 \cdot 2\pi n_e V \ln(\rho_2/\rho_1)$.

From Fig. 3 one can see that in the case of collisions with electrons at rest (without their proper thermal motion) the magnetic field suppresses by a factor of two the energy transfers at impact parameters exceeding V/ω_L (where $\omega_L = eB/mc$ is the frequency of electron revolution in the magnetic field B). This is because the electrons are capable of free motion only along the magnetic field and the averaging of energy transfers over the electrons located at identical distances ρ from the trajectory, but with different azimuthal angles, suppresses the transfer of energy from the proton to an electron in proportion to $\langle\cos^2\varphi\rangle$, where φ is the angle between the momentum transferred from the proton and the magnetic field. In the case of a longitudinal drag force, when the proton moves along the magnetic field, i.e. the angle $\varphi = \pi/2$, such suppression is quite significant, as one can see from Fig. 4. As the magnetic field B increases, the range of impact parameters within which there exist noticeable momentum transfers decreases rapidly.

Thus, in the case of an electron beam with zero temperature the magnetic field only reduces the drag force by hindering the motion of electrons. When the electrons have a noticeable velocity owing to the transverse temperature ($V_{e\perp} \gg V$), the energy transfer in the region of small impact parameters ($\rho \ll V_{e\perp}/\omega_L$), where the magnetic field is insignificant, becomes small. The contribution to the drag force from the region of large impact parameters remains the same as in the case of an electron beam with zero temperature (see the curve in Fig. 3, computed for the transverse electron velocity $V_{e\perp} = 10^7$ cm/s, which corresponds to $\rho_L = 5.6 \times 10^{-4}$ cm). The magnetic field conserves large

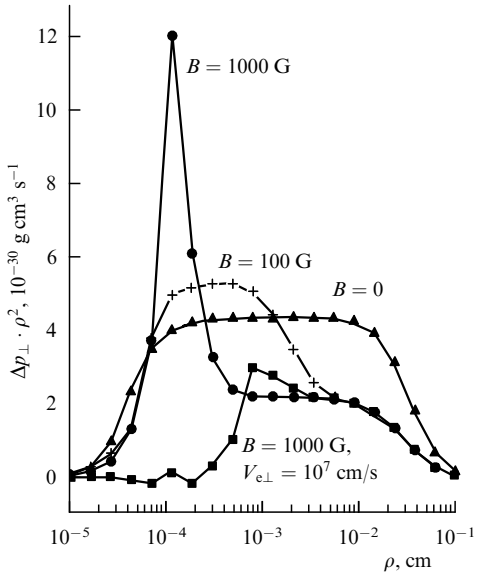

Figure 3. Contribution of collisions with electrons to the drag force versus the impact parameter in the case of motion transverse to the magnetic field. The momentum transfers for an electron beam of zero temperature are shown for various magnetic fields, as well as the influence of the transverse electron velocity at $B = 1000$ G. The proton velocity $V = 3 \times 10^6$ cm/s, the interaction time with the electron beam $\tau = 4 \times 10^{-8}$ s.

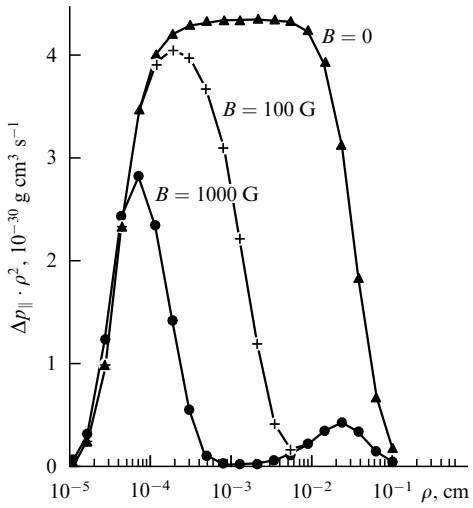

Figure 4. Contribution of collisions with electrons to the drag force versus the impact parameter in the case of motion along the magnetic field. The proton velocity $V = 3 \times 10^6$ cm/s, the interaction time $\tau = 4 \times 10^{-8}$ s.

energy transfers within the range of impact parameters from 5×10^{-4} up to 3×10^{-2} cm. As a result, the drag force for small proton velocities in the presence of a magnetic field turns out to be many times higher than without the magnetic field, and it depends weakly on the velocity of transverse electron motion.

For an ideally 'magnetized' electron beam (i.e. without electron motion transverse to the magnetic field), the drag force computed in Ref. [9] has the form

$$F_{\parallel} = -\frac{2\pi Z^2 e^4 n_e \ln(\rho_{max}/\rho_{min})}{m} \frac{3V_{\perp}^2}{|V|^5} V_{\parallel}, \qquad (12)$$

$$F_{\perp} = -\frac{2\pi Z^2 e^4 n_e \ln(\rho_{max}/\rho_{min})}{m} \frac{V_{\perp}^2 - 2V_{\parallel}^2}{|V|^5} V_{\perp}, \qquad (13)$$

where $V_{\parallel}$ and $V_{\perp}$ are the respective proton velocity components along and across the magnetic field. The drag force thus computed can be seen to 'drop to zero' when the particle travels along the magnetic field ($V_{\perp} = 0$).

The drag force in finite magnetic fields was calculated with the aid of a computer program taking into account the transverse motion of electrons. A proton ($Z = 1$) that lands in the electron beam travels with a constant velocity V in the electron gas during its time of flight τ through the electron cooler: $\mathbf{x} = \mathbf{x}_0 + \mathbf{V}t$, where $0 < t < \tau$. The motion of electrons is computed with the aid of a fourth-order Runge–Kutta method taking into account the magnetic field and the field of the moving proton. The variation of the proton momentum is computed as an integral of the interaction force taken within the time τ:

$$\Delta p = \int e^2 \left(\frac{\mathbf{x} - \mathbf{x}_{e0}}{|\mathbf{x} - \mathbf{x}_{e0}|^3} - \frac{\mathbf{x} - \mathbf{x}_e(t)}{|\mathbf{x} - \mathbf{x}_e(t)|^3} \right) n_e \, dv \, dt, \qquad (14)$$

where $n_e \, dv$ is the number of electrons in a small volume element dv.

The first term, which is determined by the initially fixed electron locations $\mathbf{x}_{e0}$, certainly turns into zero upon integration over the entire volume but, when numerical integration is performed, its use improves the computation accuracy when a finite number of summation points is used in evaluating the integral.

In the region of not too large impact parameters ρ, the actual interaction time $\tau_i = \rho/V$ of a proton with an electron is significantly shorter than the total time τ of flight across the electron cooler in the co-moving frame of reference. In a time τ_i, the electrons are shifted by $\Delta x_e \approx e^2\tau_i^2/m\rho^2 \approx e^2/mV^2 = \rho_{min}$, while the contribution of such electrons to the change in the proton momentum equals $\Delta p \approx (e^2 \Delta x_e/\rho^3)\tau_i$. The drag force created by electrons from this region can be written as

$$F = \int_{\rho_{min}}^{\rho_{max}} \frac{\Delta p}{\tau_i} n_e \cdot 4\pi\rho^2 \, d\rho = \frac{4\pi e^4 n_e}{mV^2} \ln \frac{\rho_{max}}{\rho_{min}}. \qquad (15)$$

In the case of large impact parameters, when the collisions actually do not have sufficient time to finish due to the finite time interval for which the proton is found in the cooling zone ($\rho > V\tau = \rho_{max}$), the displacements of electrons decrease rapidly: $\Delta x_e \approx e^2\tau^2/m\rho^2 \approx \rho_{min}(\rho_{max}/\rho)^2$, which improves the convergence of the integration procedure and permits the restriction of the integration to impact parameters ρ that are not too large ($\rho > \rho_{max}$).

Figures 5, 6 show the drag forces computed without a magnetic field ($B = 0$), and in the presence of various magnetic fields (the B values from 1 up to 2000 G are indicated alongside the curves), as well as the drag force computed in accordance with formulae (12), (13) for the perfectly 'magnetized' case ($B = \infty$). As the magnetic field is built up, the drag force curves are seen to converge asymptotically to a certain 'fit' curve that differs noticeably from the curve computed using formulae (12), (13).

For describing the drag force in real experiments, it is convenient to have an analytical expression that makes possible numerical computations for comparison with experimental results. Reflections on this issue have resulted in a drag force determined by the formula

$$F = -\frac{4Z^2 e^4 n_e V}{m(V^2 + V_{eff}^2)^{3/2}} \ln \frac{\rho_{max} + \rho_L + \rho_{min}}{\rho_L + \rho_{min}}, \qquad (16)$$

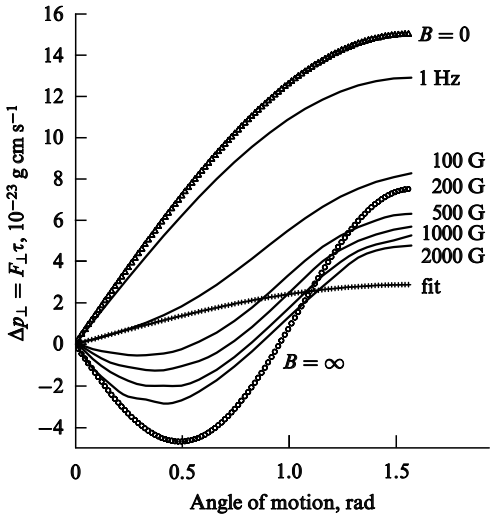

Figure 5. Component of the drag force perpendicular to the magnetic field versus the angle between the proton motion and the magnetic field: $V = 3 \times 10^6$ cm s^{-1}, $n_e = 10^7$ cm^{-3}, and $\tau = 3 \times 10^{-8}$ s.

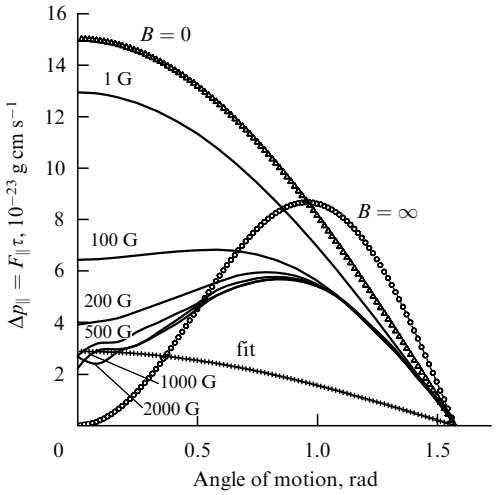

Figure 6. Component of the drag force parallel to the magnetic field versus the angle between the proton motion and the magnetic field: $V = 3 \times 10^6$ cm s^{-1}, $n_e = 10^7$ cm^{-3}, and $\tau = 3 \times 10^{-8}$ s.

where $V_{\rm eff}$ is the effective velocity of motion of Larmor circles related both to longitudinal electron velocities and to transverse drift motions caused by magnetic and electric fields owing to the space charge of beams and to inaccuracies in the creation of the concomitant magnetic field.

The argument of the logarithm makes it possible to extend application of the expression for the drag force to parameter ranges that are clearly not logarithmic. Thus, at small velocities of motion, when $\rho_{\rm min} = e^2/mV^2 \gg \rho_{\rm max} = V/\omega_{\rm e} \gg \rho_{\rm L}$ for the electron gas with zero temperature ($V_{\rm eff} = 0$), the drag force assumes the form

$$F = -\frac{(Ze)^2 n_{\rm e}^{2/3}}{c(\pi n_{\rm e}^{1/3} r_{\rm e})^{1/2}}\, V \qquad (17)$$

that is close to the results of measurements performed with the MOSOL setup [11]. These measurements revealed that the drag force is built up linearly up to its maximum $e^2 n_{\rm e}^{2/3}$ as the proton velocity increases up to $V \approx c(\pi n_{\rm e}^{1/3} r_{\rm e})^{1/2}$, after which it drops in accordance with formula (16).

If $\rho_{\rm L} > \rho_{\rm max}$, expression (16) provides a good description of the results obtained at the NAP-M facility, when partial 'magnetization' of the electron beam was observed. In this case, the drag force

$$F \propto \frac{1}{V^2} \ln \frac{\rho_{\rm max} + \rho_{\rm L}}{\rho_{\rm L}} \propto \frac{1}{VV_{\rm e}}\,,$$

i.e. it decreases with the proton velocity as V^{-1}, instead of the dependence V^{-2} expected for a zero electron temperature.

The 'fit' curves in Figs 5, 6 show the drag force computed in accordance with Eqn (16) for a magnetic field $B = 2000$ G. The values of the force obtained by computer calculations tend towards these curves. We note that the energy losses occurring in the case of motion in an electron flux $\mathrm{d}E/\mathrm{d}t = FV$ are the losses that actually have significance for electron cooling. The drag force component transverse to the velocity, which causes negative values of $F_\perp$ at small angles, is equivalent to the action of a weak transverse magnetic field and introduces no change to the damping. Figure 7 shows the energy loss due to the drag friction for various angles between the proton motion and the magnetic field. It can be seen that calculations using formulae (12), (13) yield an exaggeratedly strong influence of the angle of proton motion, while the model for the drag force (16) is in reasonable agreement with numerical computations.

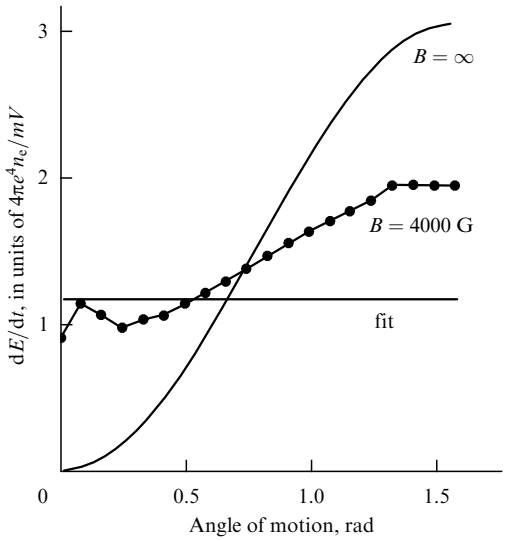

Figure 7. Energy loss due to the drag friction in the perfectly 'magnetized' case ($B = \infty$), for the drag force model (16) denoted as 'fit', and the results of numerical calculations (dots) versus the angle of proton motion relative to the orientation of the magnetic field.

2.3 Stationary parameters of an ion beam after cooling

Cooling of the ion beam continues until equilibrium is established between the heating (energy supply) and cooling (energy extraction) processes. The main source of heating at a low intensity of the ion beam is diffusion caused by random kicks received by the ions owing to the thermal motion of the beam electrons:

$$\frac{\mathrm{d}p^2}{\mathrm{d}t} = \frac{4\pi Z^2 e^4 n_{\rm e} L_{\rm c}}{V_{\rm eff}}\,, \qquad (18)$$

where $V_{\rm eff}$ is the effective electron velocity.

The equation of balance between cooling and heating in the spherically symmetric case (without a magnetic field, when $V_{\rm eff}$ is determined by the ion temperature) has the form

$$\frac{\mathrm{d}p^2}{\mathrm{d}t} = 2\langle \mathbf{p}\cdot\mathbf{F}\rangle_{\rm cool} + \left(\frac{\mathrm{d}p^2}{\mathrm{d}t}\right)_{\rm heat} = -AM\frac{4\pi Z^2 e^4 n_{\rm e} L_{\rm c}}{mV_{\rm eff}^3}\langle V^2\rangle + \frac{4\pi Z^2 e^4 n_{\rm e} L_{\rm c}}{V_{\rm eff}}\,, \qquad (19)$$

where A is the ion mass in the atomic mass units M. Equation (19) is seen to lead to a simple condition for equalization of the ion and electron beam temperatures:

$$\langle V^2\rangle = \frac{m}{AM}\, V_{\rm eff}^2\,, \quad T = T_{\rm e}\,. \qquad (20)$$

In a strong magnetic field, the effective motion of Larmor circles in an ideal cooler (the magnetic field lines are parallel to the orbit of the ion beam) depends only on the longitudinal repulsion between the electrons distributed randomly in space after acceleration. The effective electron temperature can be estimated by the formula [11]

$$T_{\rm eff} = \frac{mV_{\rm eff}^2}{2} = \frac{AM\langle V^2\rangle}{2} \approx 2e^2 n_{\rm e}^{1/3}\,. \qquad (21)$$

When the electron beam density $n_{\rm e} = 10^8$ cm^{-3}, this estimation yields the value $T_{\rm eff} \approx 1$ K, and in many devices, starting from NAP-M [12], such low temperatures were actually achieved for the longitudinal motion of ions.

For the transverse motion of ions in a storage ring there exist additional heating factors (especially, in the case of positively charged ions) due to the formation of quasi-recombined weakly bound electron – ion pairs in the cooling zone, which break up upon exit from the electron cooler. Here, a strong magnetic field acts on the electron, thus resulting in additional diffusion due to the randomness of the moment when the electron is captured by ions entering the electron beam.

However, the strongest additional heating in the transverse direction is due to the influence of machine resonances. The field of the cooled ion beam space charge results in a shift

and spread of the frequency of betatron oscillations, and the largest possible shift $\Delta\nu_{\max}$ serves as a good characteristic. At the same time, the smallest transverse emittance achievable in cooling is limited by the value

$$\epsilon = \frac{\sigma_\perp^2}{\beta_\perp} = \frac{NRr_i}{\pi l_b \beta^2 \gamma^3 \Delta\nu_{\max}}, \quad (22)$$

where l_b is the length of the ion bunch, $r_i = (Ze)^2/AM$ is the classical ion radius, $\beta_\perp$ is the beta function, and R is the average radius of the storage ring.

Experiments have revealed that the most typical frequency shift of betatron oscillations, obtained in conditions of electron cooling, amounts to $\Delta\nu_{\max} \approx 0.1-0.2$. Usually, the ion beam size decreases until the frequency shift of betatron oscillations reaches the values indicated. In the case of large ion currents, this allows reliable estimation of the transverse sizes of the ion beam in setups lacking devices for measuring the ion beam profile.

Ion scattering within the beam is a factor determining the longitudinal momentum spread in the beam for ion currents that are not too small. As a rule, the decrement of longitudinal cooling is significantly higher than the transverse one and, consequently, the longitudinal spread of ion momenta is significantly lower in the co-moving frame of reference than the lateral spread.

As a result, the mutual scattering of ions leads to an enhancement of the longitudinal momentum spread at a rate

$$\frac{d}{dt}\left(\frac{\Delta p_\parallel}{p}\right)^2 = \frac{4r_i^2 N c L_c}{\gamma^3 \epsilon^{3/2}\sqrt{\beta_\perp}}. \quad (23)$$

As the number of particles N in the ion beam increases, the longitudinal momentum spread increases quite weakly, since the transverse emittance of the beam increases in accordance with Eqn (22). But such simple thermodynamics is observed in a cooled beam only in the case of sufficiently high temperatures, when correlations between the locations of adjacent particles can be neglected.

3. Features peculiar to the dynamics of a cold ion beam

3.1 The dynamics of longitudinal motion in a cold ion beam

A strongly cooled ion beam is an interesting and quite promising object for accelerator science and for certain applications. In the case of an intense beam, a situation may be realized when after cooling the azimuthal velocity of thermal motion of the particles along the beam, characterized by the spread of angular frequencies of revolution, $d\theta/dt = \Delta\omega$ (in rad s^{-1}), becomes significantly lower than the angular velocity Ω of coherent wave propagation along the beam azimuth [13] with

$$\Omega^2 = \frac{Nr_i \eta c^2 L_b}{\gamma^3 \cdot 2\pi R^3}. \quad (24)$$

Here, $\eta = (d\omega_0/dp)(p/\omega_0)$ is the coefficient of the revolution frequency dependence upon the momentum, $L_b = 1 + 2\ln(b/a)$ is the logarithm determining the beam potential (b/a is the ratio of the chamber radius to the beam radius). In this event the model of an ideal gas of non-interacting ions is not adequate to the actual behavior of the beams: strong correlations arise in the mutual positions of ions.

Usually, instabilities develop in accordance with the so-called Keil–Schnell criterion, and it seems to be impossible for beams to exist stably in the presence of resonances in longitudinal impedance Z/n and currents that do not exceed the limit determined by the expression

$$I < \frac{|\eta|(E/e)(\beta\Delta p/p)^2}{|Z/n|}. \quad (25)$$

In the case of a storage ring with a chamber that is a good conductor, the longitudinal impedance $Z/n = L_b/(c\beta\gamma^2)$, which was used in writing down Eqn (24). In this case, the stability condition (25) can be represented in a simple form: $\Delta\omega^2 > |\Omega^2|$.

But if one considers an ion beam travelling with a velocity noticeably lower than the speed of light, then its interaction with the high-frequency elements of the vacuum chamber is suppressed, while the low-frequency elements (such as resonators) can be reliably shunted. When working at an energy below the critical energy for removing the negative mass effect and self-bunching of the ion beam, it turns out to be possible to achieve experimentally a stable state of an ion beam with a temperature that is hundreds of times lower than that admissible by the formal stability criterion.

The interaction occurring inside an ion beam is most conspicuous in the strong change in the shot noise of the beam. If the ion temperature is sufficiently high, each individual ion travels along an ion column independently of the other ions and during its flight past the electrode it induces at the measuring pickup electrodes a periodic signal in the form of a short bump of voltage. With the aid of a periodic delta-function $\delta(\theta)$, the total signal proportional to the ion density at a point with the beam azimuth θ can be written as

$$\rho(\theta, t) = \sum_{k=1}^{N} \delta\big(\theta - \theta_k(t)\big) = \frac{1}{2\pi}\sum_{n=-\infty}^{\infty} A_n(t)\exp(in\theta). \quad (26)$$

The amplitude $A_n(t)$ of the nth density harmonic is defined as

$$A_n(t) = \sum_{k=1}^{N} \exp\big[-in\theta_k(t)\big], \quad (27)$$

where $\theta_k(t)$ is the azimuthal position of the kth ion. If the ions in the beam travel freely and $\theta_k = \theta_{k0} + \omega_k t$, then the signal spectrum around the nth harmonic of the revolution frequency reflects the momentum distribution $f(\Delta p)$ of particles, since $\Delta\omega_k = \omega_0\eta(\Delta p/p)_k$ (where ω_0 is the revolution frequency in the storage ring). The integral of the spectrum around the nth harmonic (or the power of the signal at the pickup electrode) is proportional to the beam current, viz.

$$\frac{1}{2\pi}\int W(\omega)\,d\omega = \langle A_n^2(t)\rangle = N. \quad (28)$$

This is the so-called Schottky noise of the particle beam (the shot noise).

When the ion beam intensity becomes high, the motion caused by the field of a particular ion in the other particles of the beam influences the noise spectrum significantly. The

potential energy of an ion beam density fluctuation with the amplitude A_n in the co-moving frame of reference is given by

$$E_{\rm p} = \frac{(Ze)^2 A_n^2 L_{\rm b}}{4\pi R\gamma} \,. \tag{29}$$

The temperature related to the kinetic energy of the ion motion is determined by the expression

$$\frac{kT}{2} = \frac{M_{\rm s}\Delta V_{||}^2}{2} = \frac{M\Delta\omega^2 R^2\gamma^2}{2\eta} \,. \tag{30}$$

Here, $M_{\rm s} = MA/\eta$ is the effective mass of the longitudinal motion of ions along the beam with due regard for the focusing effect in the storage ring.

In the case of a beam of low intensity, the distribution over the amplitudes A_n exhibits a purely statistical character and has a Gaussian shape with a variance N:

$$f(A_n) \propto \exp\left(-\frac{A_n^2}{2N}\right) .$$

For high beam intensity, it is necessary to take into account the Boltzmann distribution over the fluctuation energy, $\exp(-E_{\rm p}/kT)$, when the potential energy of the fluctuation, $E_{\rm p}$, becomes significant compared to the energy of thermal motion:

$$\begin{aligned} f(A_n) &\propto \exp\left(-\frac{A_n^2}{2N}\right)\exp\left(-\frac{A_n^2}{N(\Delta\omega/\Omega)^2}\right) \\ &= \exp\left[-\frac{A_n^2}{2}\left(\frac{1}{N}+\frac{1}{N_{\rm th}}\right)\right], \end{aligned} \tag{31}$$

where

$$N_{\rm th} = N\frac{\Delta\omega^2}{2\Omega^2} = \frac{\pi\eta(\Delta p/p)^2 R\beta^2\gamma^3}{r_{\rm i}L_{\rm b}} \,. \tag{32}$$

When the number of particles is large, the dispersion $\langle A_n^2\rangle$ of the harmonics (or, which is the same, the integral of the power spectrum around the nth harmonic) is limited by the threshold number $N_{\rm th}$ and, as seen from Eqn (31), equals

$$\langle |A_n|^2\rangle = \frac{NN_{\rm th}}{N+N_{\rm th}} \,. \tag{33}$$

We here draw attention to the fact that when the storage ring operates at an energy exceeding the critical energy and $\eta < 0$, the threshold number $N_{\rm th}$ is negative, and in the case of a large number of particles the amplitude of fluctuations increases. This is a manifestation of the so-called negative mass instability and of beam self-bunching that occurs as $N + N_{\rm th}$ approaches zero.

The threshold number $N_{\rm th} \propto \Delta\omega^2$ can be seen to be large ($N_{\rm th} \gg N$) and the power of the beam noise proportional to N if the beam is hot. As indicated above, this is the ordinary Schottky noise. On the contrary, in the case of strong cooling the threshold number $N_{\rm th}$ becomes significantly smaller than the number N of particles in the ion beam, and the beam noise becomes thermal noise when the power is independent of the current, but is determined only by the beam temperature (proportional to the spread squared of revolution frequencies $\Delta\omega^2$).

Under the action of electron cooling, the longitudinal momentum of particles fluctuates around the equilibrium value, and the characteristic time required for the momentum to change value is $1/\lambda$ (λ is the cooling decrement). In the situation of a small dispersion and strong damping ($\Delta\omega/\lambda \ll 1$) ions start undergoing diffusive motion along the beam: a particle covers a small part of the perimeter $\Delta\theta = \Delta\omega/\lambda$, upon which its velocity of motion changes significantly. As a result, the position of the particle fluctuates randomly around its initial position and the dispersion of its displacement along the beam increases with time t as $\langle\Delta\theta^2\rangle^{1/2} = (\Delta\omega^2 t/\lambda)^{1/2}$. This leads to the effective deceleration of the particle motion along the beam and to a strong narrowing of the noise spectrum in the vicinity of harmonics of the revolution frequency.

The effects described above can be simulated relatively simply with a computer by the method of quasi-particles travelling along the beam in accordance with the drag force and the resulting space charge fields. Figure 8 shows how the noise spectrum of the beam, obtained by computer simulation, varies with the cooling decrement. The spectrum can be seen to change from being practically a Gaussian (a parabola in logarithmic representation) to becoming narrow (with a width $\delta\omega \approx \Delta\omega^2/\lambda$) when the cooling decrement significantly exceeds the thermal spread of revolution frequencies.

Interaction between particles in an intense beam substantially alters the shape of the spectrum. In this event density fluctuations along the ion beam propagate in the form of a wave with azimuthal velocity Ω depending on the beam density, but not on the thermal velocities (proportional to $\Delta\omega$). In the case of a high beam intensity N, when $\Omega > \Delta\omega$, the spectrum at the nth harmonic splits into two peaks ($\pm n\Omega$) corresponding to space charge waves running along and against the beam propagation (Fig. 9).

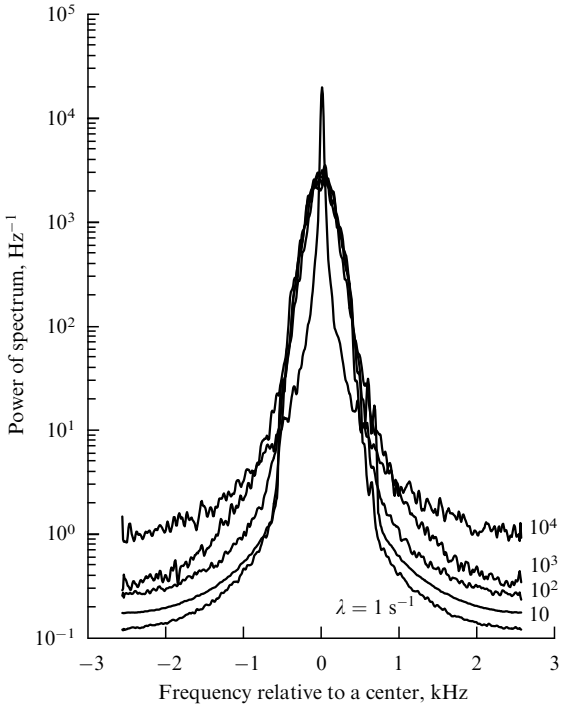

Figure 8. Beam noise spectra for cooling decrement λ increasing from 1 up to 10^4 s^{-1}. The number of particles in the beam $N = 10^6$, the thermal spread of revolution frequencies $\Delta\omega = 1000$ s^{-1}.

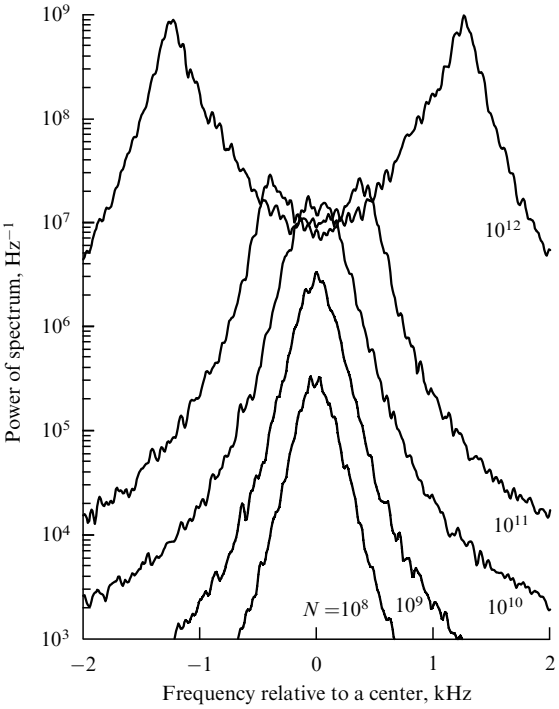

Figure 9. Beam noise spectra for number of particles in the beam N increasing from 10^8 up to 10^{12}. The cooling decrement $\lambda = 10^3\ \mathrm{s}^{-1}$, the thermal spread of revolution frequencies $\Delta\omega = 1000\ \mathrm{s}^{-1}$.

Figure 10 presents the noise spectrum of a beam of argon $^{40}_{18}\mathrm{Ar}^+$ ions measured at the heavy-ion synchrotron SIS. The structure of the spectrum is clearly seen with two peaks around the harmonic of the revolution frequency. Such measurements permit data on the beam momentum spread and on the cooling decrements to be obtained by comparison with computed spectra.

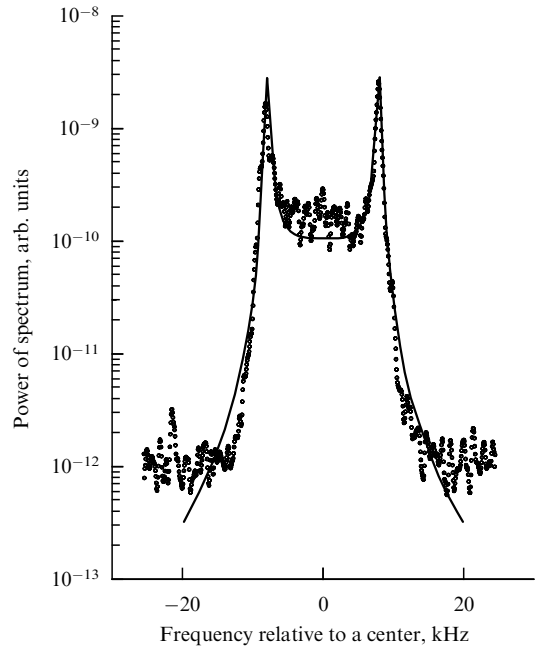

Figure 10. Noise spectrum of a beam of $^{40}_{18}\mathrm{Ar}^+$ ions with a current of 4.4 mA around one of the harmonics of the revolution frequency (35 MHZ) at the SIS facility in the case of cooling by a 400-mA electron current. Solid line illustrates the shape of the spectrum at $\Delta p/p = 1.1 \times 10^{-4}$ and was calculated using Eqn (34). The cooling decrement $\lambda = 10^3\ \mathrm{s}^{-1}$.

Assuming the particle momenta to exhibit a Gaussian distribution, the expression obtained in Ref. [13] for the spectra has the form

$$W(\omega) = GN\left(\frac{\Delta\omega}{\Omega}\right)^2 \frac{2\,\mathrm{Im}\,\epsilon(\omega)}{\omega|\epsilon(\omega)|^2}\,. \tag{34}$$

Here, G is a constant of the amplification path of the measuring pickup electrode, $\omega = 2\pi(f - nf_0)$ is the frequency relative to the nth harmonic, and $\epsilon(\omega)$ is the dielectric constant of the ion beam defined as

$$\epsilon(\omega) = 1 + \left(\frac{\Omega}{\Delta\omega}\right)^2 \left[1 + \frac{\mathrm{i}\omega}{\lambda q - \mathrm{i}\omega}\left(1 + \frac{q}{1+q-\mathrm{i}\omega/\lambda} + \ldots + \frac{q^m}{(1+q-\mathrm{i}\omega/\lambda)\ldots(m+q-\mathrm{i}\omega/\lambda)} + \ldots\right)\right],$$

where $q = (n\Delta\omega/\lambda)^2$.

The solid line in Fig. 10, calculated in accordance with formula (34), shows a good agreement between calculations and measurements. The data obtained from measurements at different harmonics of the revolution frequency permit one to reliably extract the decrements of longitudinal cooling and the momentum spreads at equilibrium. The momentum spread for a strongly cooled beam is not determined from the width of the spectrum, but from the power of the signal at the pickup electrodes in accordance with Eqns (32), (33).

3.2 Problems in obtaining 'crystalline beams'

The strong suppression of noise signals, manifested both in a reduction in the power of noises and in the appearance of a double-peak structure, takes place simultaneously at all harmonics of the revolution frequency, for which the wavelength is greater that the transverse dimension of the vacuum chamber. What happens at very small distances, and are beam states feasible in which there are mutual correlations between adjacent particles? Actually, such states are a transition between the models of an ideal gas and of a liquid.

An interesting phenomenon was observed in experiments at NAP-M — strong suppression of scattering inside the beam at small proton currents. Figure 11 shows the behavior of the shot noise power of the proton beam in the case of cooling with an electron beam and in the absence of cooling [12]. After cooling the shot noise of the beam is seen to be reduced by two orders of magnitude for a proton beam current of 10 μA (the number of protons in the beam $N = 10^7$), which corresponds to transformation of the shot noise into thermal noise proportional to the longitudinal temperature of the beam. The fact that the noise power is constant within the 0.1 – 10 μA range of currents indicates that the longitudinal temperature in the co-moving frame of reference is constant and about 1 K, which corresponds to a momentum spread of $\Delta p/p = 10^{-6}$.

Internal scattering in a strongly cooled beam usually determines the momentum spread established during the cooling process. In the case of proton currents within the 0.1 – 10 μA range, the transverse beam dimension varied little, and the established momentum spread should have amounted to at least $\Delta p/p \approx (5 - 50) \times 10^{-6}$, even if the

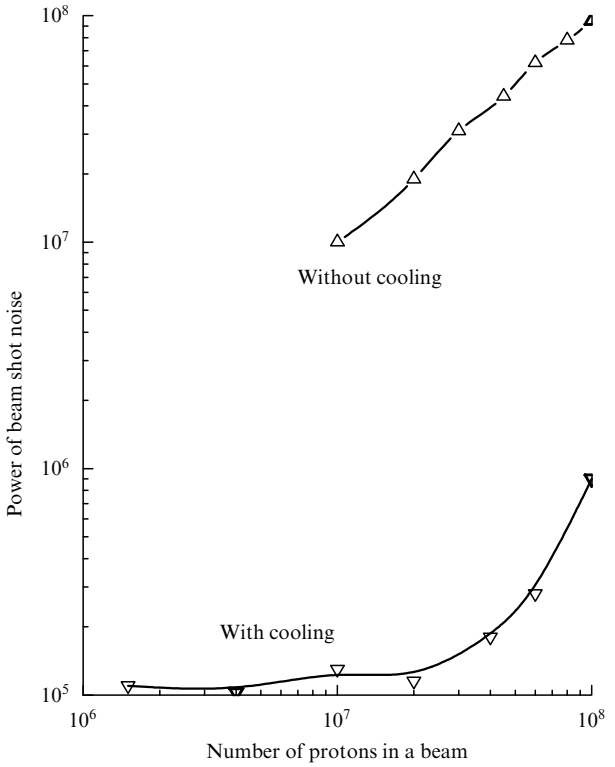

Figure 11. Power of current fluctuations of the proton beam (normalized to the power of the signal due to a single proton) versus the proton current of the beam at the NAP-M storage ring without cooling and with cooling by a 0.3-A electron current (energy 65 MeV).

longitudinal decay time was assumed to equal 1 ms. The momentum spread obtained (50 times smaller than expected) could be related to a manifestation of ordering at the level of neighboring particles, when the particles undergo mutual longitudinal oscillations, but do not slip past each other along the orbit. In this case, energy transfer from transverse to longitudinal motion is strongly suppressed.

Later, similar effects were observed at the ESR facility with electron cooling of heavy ions, when the momentum spread varied weakly provided the number of particles was small, and, then, as the number of particles reached a certain critical value, it underwent a steplike enhancement [14]. Figure 12 displays an example of such measurements for gold ions cooled at the ESR facility by an electron current of 250 mA.

For testing the model one can attempt to apply expression (23) for the rate of the longitudinal momentum spread due to scattering inside the beam, multiplied by $\exp(-E_i/kT_\parallel)$, so as to take into account suppression of the mutual slipping of particles in the orbit thanks to the existence of the potential barrier E_i. Here, the energy of the potential barrier is assumed to be determined by the transverse dimension $a_\perp$ of the ion beam:

$$E_i = \frac{(Ze)^2}{a_\perp} - \frac{(Ze)^2}{a_\perp + \Delta s}\,,$$

where $\Delta s = P/N$ is the longitudinal distance between the ions ($P = 2\pi R$ is the perimeter of the storage ring).

Figure 13 presents an example of the momentum spread calculated for the ESR facility. The result of calculation is

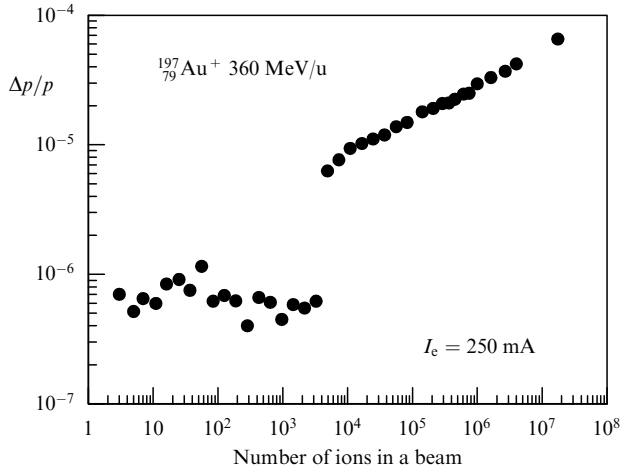

Figure 12. Momentum spread versus number of $^{197}_{79}Au^+$ ions, measured at the ESR facility of GSI (the figure was kindly presented by M Steck).

seen to be very close to the momentum spread actually examined experimentally, so the hypothesis that there is a correlation among the longitudinal positions of ions at small ion currents seems reasonable.

The results presented above stimulated investigations of the possibilities for obtaining crystalline states of beams in ion storage rings. In principle, such states are observed in traps with laser cooling, when the ions are at rest relative to the trap [15, 16]. The creation of truly crystalline beam states (in all three dimensions) in storage rings is hindered by their destruction during motion in the storage ring. This is reminiscent of attempts to roll a crystal trough the rollers of a forming mill which deforms the crystal in the transverse direction, naturally ending in destruction of the crystal.

The field of the space charge defocuses the ions in the transverse direction and, in accordance with Eqn (22), the

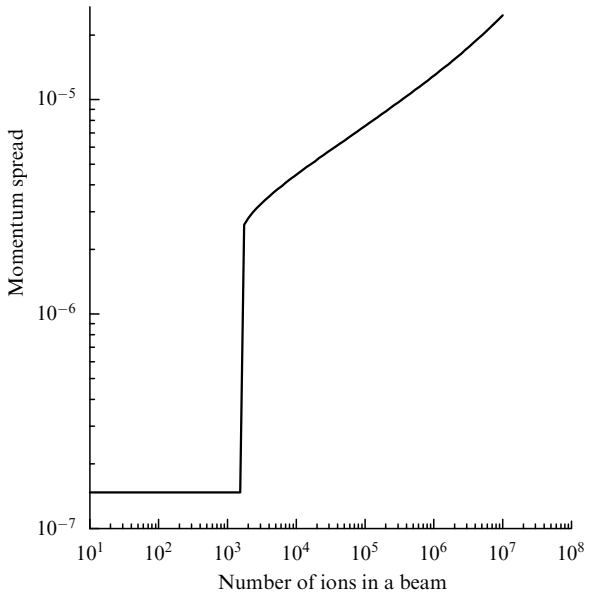

Figure 13. Momentum spread versus the number of $^{197}_{79}Au^+$ ions with account taken of correlations inside the beam (under conditions of measurements at the ESR facility, presented in Fig.12).

frequency shift of betatron oscillations amounts to

$$\Delta\nu = \frac{\pi n_i r_i R^2}{\beta^2\gamma^3 v}\,. \tag{35}$$

The characteristic distance between ions is $\Delta a \approx n_i^{-1/3}$, and the parameter determining the excess of interaction energy over the temperature can be written in the form

$$\Lambda = \frac{(Ze)^2}{kT\Delta a}\,.$$

In a perfect crystal, the ions do not move relative to each other but, owing to thermal motion, undergo small oscillations of amplitude $\delta a \approx \Delta a/\Lambda$ in the ion lattice. Clearly, one can speak of a crystal lattice only if the condition $\Lambda \gg 1$ is satisfied. In the opposite case ($\Lambda \ll 1$), the interaction between particles can be neglected and the beam size will depend on the external focusing and temperature T. When $\Lambda \gg 1$, the external focusing is compensated by internal repulsion and the ions oscillate relative to their shifted position inside the 'crystal' instead of the orbit center.

It is still not clear, how the transition from a disordered state to a three-dimensional crystalline structure can take place, given the very strong frequency shift of betatron oscillations required. Many theoretical publications [15], in which various versions of focusing and three-dimensional structures such as embedded spirals are analyzed, have been devoted to this issue. However, a three-dimensional crystal in an accelerator has yet to be obtained, although facilities for implementing this beautiful idea are being created [16].

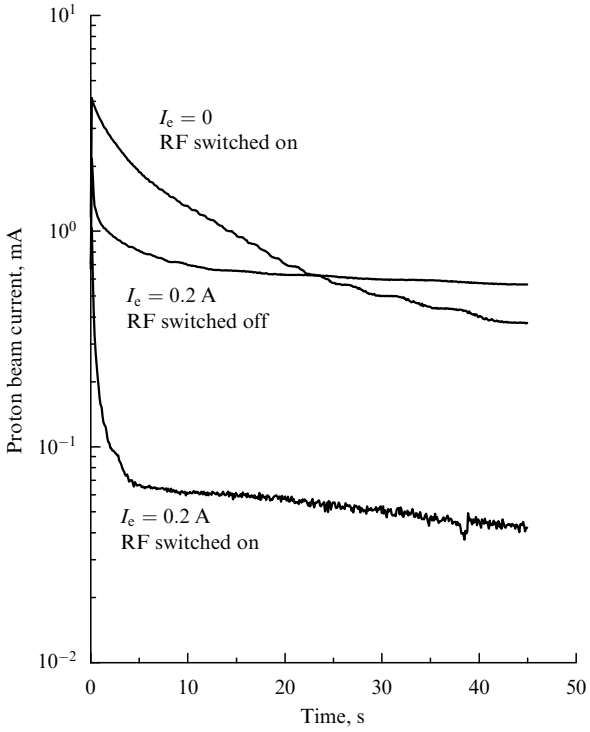

Figure 14. Dependence of proton beam current upon the time that passes after beam injection into the CELSIUS storage ring without cooling ($I_e = 0$) and in the case of cooling with an electron current $I_e = 0.2$ A with the RF voltage across the accelerating cavity switched on and off.

4. Effects due to the interaction of beams in the case of electron cooling

4.1 Experiments with the cooling of an intense ion beam

The utilization of electron cooling for ion beams of high intensity has revealed that strong losses of the ion beam occur at the initial stages of cooling. The CELSIUS storage ring with electron cooling was one of the first facilities where this phenomenon was most conspicuous [17]. However, strong losses of intense ion beams also took place at other facilities [18, 19].

In the CELSIUS storage ring, an injection is applied that involves the charge exchange of hydrogen ions H_2^+ leaving the cyclotron with an energy of 96 MeV. The large breakup cross section of the H_2^+ ion into protons of energy 48 MeV permits the aperture of the storage ring to be filled with a proton beam practically up to the limit with respect to the space charge (15–30 mA). Attempts at cooling a proton beam of such intensity gave rise to very rapid losses of intensity, and only 30–100 μA were cooled into a thin beam, as shown in Fig. 14.

The cooling of a proton beam distributed uniformly along its orbit (with the RF voltage across the accelerating cavity switched off) noticeably enhanced the average current that remained after cooling. Cooling with the RF voltage across the accelerating cavity switched on led to the protons grouping into a short bunch, accompanied by a sharp increase in the beam pulse current as compared to the average value. Measurements showed that limits were imposed precisely on the instantaneous (pulse) current of the proton beam; the RF voltage being switched on resulted in a drastic decrease in the average current (see Fig. 14).

When H^+ (instead of H_2^+) ions were accelerated in the cyclotron, it was possible to obtain a noticeably higher energy; in this case, however, the possibility of charge exchange injection vanished, and during a single pulse only a 50–100-μA proton current at an energy of 180 MeV could be injected into CELSIUS. Electron cooling resulting in compression of the proton beam from a size of several centimeters down to 1 mm allowed such injections to be performed repeatedly, thus accumulating proton current.

From Fig. 15 it is seen that whereas accumulation is linear in time in the case of small proton currents, the losses between injections increase significantly and the accumulated current is determined by the equilibrium between new injections and these losses, when the currents amount to 3–5 mA. When new injections stop, the proton current first drops rapidly, and then more and more slowly as the current decreases. Figure 16 shows that the losses exhibit a threshold character: they arise and undergo a sharp increase when the proton current exceeds 2 mA. The size of the proton beam, measured in these experiments, amounted to 0.7 mm.

When the momentum spread is too small, cooling itself can cause the development of instabilities owing to interaction with some of the elements of the vacuum chamber. But the initial spread of the proton beam was not too large ($\Delta p/p \approx 5 \times 10^{-4}$) and after cooling it decreased to $\Delta p/p \approx 10^{-4}$. It is seen that after a reduction in the beam intensity by two orders of magnitude and a decrease in the momentum spread by a factor of only 5, longitudinal instabilities should also have been manifested more strongly without cooling.

Measurements with an electron beam in the case of strongly tuned out energy, when no cooling took place but

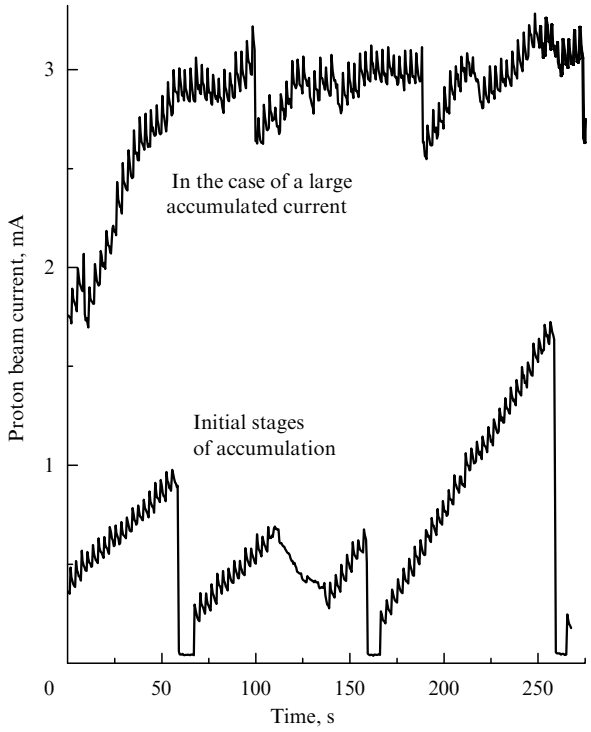

Figure 15. Several cycles of accumulation of the proton beam current in the CELSIUS storage ring in the case of electron cooling ($I_e = 1.8$ A, $E_p = 180$ MeV).

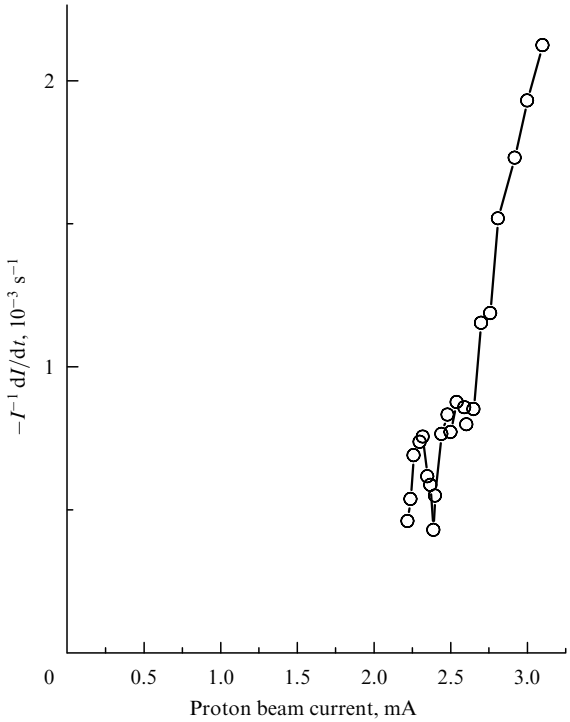

Figure 16. Dependence of proton beam current loss $-I^{-1}\,dI/dt$ on the circulating current in the CELSIUS storage ring ($I_e = 1.8$ A, $E_p = 180$ MeV).

nevertheless the proton current losses remained large, convinced the experimenters that the main cause of losses consists in the presence of electrons in the orbit of an intense proton beam.

The experience acquired from the cooling of an intense proton beam at the LEAR facility [20] with electron cooling turned out very interesting. This storage ring has a very powerful system of feedbacks used for stochastic cooling. The frequency band of the LEAR feedback system exceeds 500 MHz, and its utilization with reduced amplification factors enabled the transverse instabilities to be suppressed and the number of protons accumulated increased by two orders of magnitude — up to 8×10^{10}.

4.2 Specific features of the cooling of coherent fluctuations

Already the first studies of collective interaction in systems for electron cooling revealed that an electron beam can introduce very strong damping into the coherent oscillation modes of ion beams [21, 22]. Here, the damping constant of coherent modes rises linearly with the electron density and with the number of ions undergoing the interaction.

In a reference system concomitant to the beams, the equilibrium state of particles is determined by the joint action of the external focusing field and the field of the beam space charge. When fluctuations arise in the ion beam, an electrostatic field arises that restores the particles to the equilibrium state. Consider plasma oscillations in the ion beam, consisting in the motion of a small bunch of the ion beam containing N_i particles with respect to the main beam. The additional energy related to the interaction of this bunch and the beam amounts to

$$W = N_i \left(\frac{M_i V_i^2}{2} + \frac{M_i \omega_i^2 x_i^2}{2} \right). \tag{36}$$

In the absence of an electron beam, oscillations of an ion beam bunch occur with conservation of the total energy W: the kinetic energy transforms into potential energy and vice versa with the frequency of plasma oscillations. When an ion bunch travels within an electron beam with a velocity V_i, the variation in its position excites an electric field of intensity $E = 4\pi n_i Z e V_i \tau$. During its interaction time τ with the electron beam, this field causes the motion of electrons within the electron beam with a momentum $\Delta p = eE\tau$, which is equivalent to a loss of energy $\Delta W_k = N_e \Delta p^2 / 2m$ in the coherent ion motion.

Assuming the numbers N_i and N_e of particles participating in the interaction to be determined by the fluctuation volume v_f and the respective beam densities: $N_i = n_i v_f$ and $N_e = n_e v_f$, we obtain the (dimensionless) relative decrement of energy loss corresponding to one flight through the cooling zone in the form

$$\lambda = \frac{\Delta W_k}{M_i V_i^2 / 2 N_i} = \omega_e^2 \omega_i^2 \tau^4 , \tag{37}$$

where ω_e and ω_i are the frequencies of plasma oscillations in the electron and ion beams, respectively.

The loss of a single particle moving within an electron flow with a velocity V_i are determined [see Eqn (9)] by the drag force $F = 4\pi Z^2 e^4 n_e L_c / m V_i^2$, while the relative loss decrement for one flight through the cooling zone equals

$$\lambda_1 = \frac{F\tau}{M_i V_i} = \frac{\omega_e^2 \tau (eZ)^2 L_c}{M_i V_i^3} . \tag{38}$$

The ratio of the decrements (37) and (38) is

$$\frac{\lambda}{\lambda_1} = \frac{n_i (V_i \tau)^3}{L_c} , \tag{39}$$

and the coherent decrement exceeds the one-particle decrement by a factor equal to the number of ions present in the coherent interaction region of size $a_c = V_i\tau$.

Does coherent interaction always introduce useful damping in the ion beam or it can give rise to problems with the beam stability?

As the beam density (for instance, of the electron beam) increases, the rise in the energy loss of the coherent fluctuation due to the excitation of motion in the electron beam is limited by Debye screening [23]. When $\omega_e\tau > 1$, the ion bunch moving within the electron beam is surrounded by an electron cloud compensating the field of the ion beam space charge, and the momentum transferred to the electrons by the field of the ion fluctuation ceases to rise in proportion to τ.

The maximum energy loss experienced by a moving ion bunch that traps ZN_i electrons amounts to

$$\Delta W = -gZN_i\frac{mV_i^2}{2}\,, \tag{40}$$

where g is a factor taking into account the details of the interaction (for purely inelastic collisions $g = 1$, for elastic collisions $g = 4$).

The losses (40) extract energy from the coherent fluctuation and cause damping of its oscillations. However, compensation of the ion fluctuation field also has a negative aspect: the restoring field of ion plasma fluctuations vanishes, and the ions move freely (together with the screening electrons) while the bunch is located inside the electron beam:

$$X_{out} = X_{in} + V_{out}\tau\,,$$

$$V_{out} = V_{in} - g\frac{Zm}{2M_i}V_{in}$$

instead of

$$X_{out} = X_{in}\cos(\omega_i\tau) + \frac{V_{in}}{\omega_i}\sin(\omega_i\tau)\,,$$

$$V_{out} = V_{in}\cos(\omega_i\tau) - X_{in}\omega_i\sin(\omega_i\tau)$$

when the plasma oscillations occur outside the electron beam.

Figure 17 presents an example of free motion of ions in the cooling zone, which reveals strong enhancement of the amplitude of ion coherent oscillations after departure from the electron beam. Disruption of the interacting electron and ion beams at the moment of their departure from the cooling zone turns out to be a source of additional energy increasing the amplitude of coherent oscillations in the ion beam.

Departure of the ion fluctuation from the cooling zone leads to a change in energy per single ion equal (with account taken of $\langle V_{in}X_{in}\rangle = 0$ and $\delta V_i \ll V_i$) to

$$\frac{\Delta W}{N_i} = \left(-g\frac{Zm}{2} + \frac{M_i(\omega_i\tau)^2}{2}\right)V_i^2\,. \tag{41}$$

Here, the first term gives the dissipative losses at arrival (40), the second reflects the enhancement of the potential energy of interaction of a small oscillating ion bunch with the other ions in the beam owing to the free displacement of ions during the flight through the cooling zone. From formula (41) it is seen that the damping of coherent oscillations occurs only if the ion beam density is not too high:

$$(\omega_i\tau)^2 < g\frac{Zm}{M_i\tau}\,, \tag{42}$$

which corresponds to the largest possible coherent decrement Zm/M_i.

Introducing the frequency of electron oscillations in the field of the ion beam space charge, $\omega_{ei} = \sqrt{4\pi e^2 n_i/m} = \omega_i\sqrt{M_i/m}$, yields the simple restriction

$$\omega_{ei} < \frac{\sqrt{g}}{\tau}\,. \tag{43}$$

From this expression it follows that if the phase shift of electron oscillations in the ion beam field occurring during the interaction time τ is too strong, we will obtain instability and heating instead of cooling!

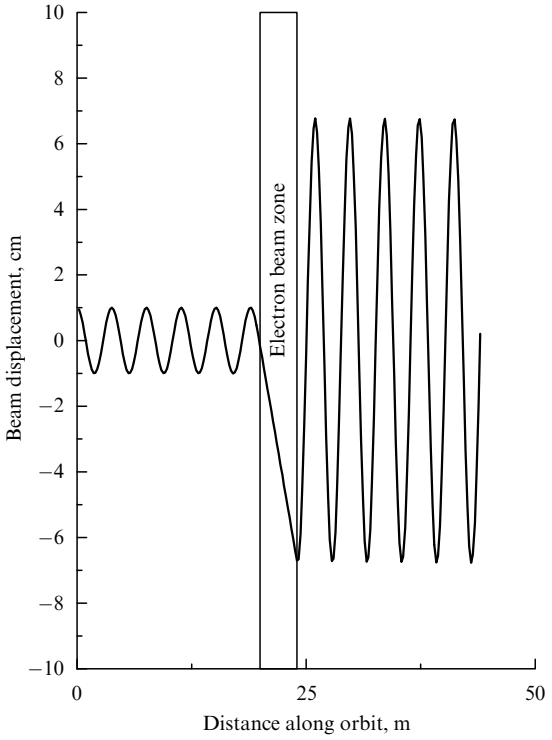

Figure 17. Change of amplitude of plasma oscillations after flight through the zone with intense electron beam.

4.3 Matrix analysis of the coherent stability of an electron cooling system

Consider the electron and ion beams in the cooling zone to be of cylindrical shape with densities n_e and n_i, respectively. We write out the equations for relative dipole oscillations within the cooling zone in the following form

$$\frac{d^2\xi_e}{dt^2} = -\omega_{ei}^2(\xi_e - \xi_i) + i\Omega_e\frac{d\xi_e}{dt}\,, \tag{44}$$

$$\frac{d^2\xi_i}{dt^2} = -\omega_{ie}^2(\xi_i - \xi_e) - i\Omega_i\frac{d\xi_i}{dt}\,, \tag{45}$$

where $\xi_e = x_e + iy_e$ and $\xi_i = x_i + iy_i$ are the respective transverse positions of the electron and ion beam centers; $\omega_{ei} = \sqrt{2\pi Ze^2 n_i/m}$ is the oscillation frequency of electrons in the field of the ion beam space charge; $\omega_{ie} = \sqrt{2\pi Ze^2 n_e/M_i}$ is

the oscillation frequency of ions in the electron beam space charge; $\Omega_e = eB/mc$ and $\Omega_i = ZeB/M_i c$ are the respective Larmor oscillation frequencies of electrons and ions with the respective masses m and M_i in a magnetic field B.

The consistent solution of the linear equations (44) and (45) with the initial conditions for the electrons $x_e(0) = 0$, $\mathrm{d}x_e(0)/\mathrm{d}t = 0$ in the cooling zone can be written as

$$\begin{pmatrix} x_i \\ \dfrac{\mathrm{d}x_i}{\mathrm{d}t} \end{pmatrix} = \begin{pmatrix} A_{11} & A_{12} \\ A_{21} & A_{22} \end{pmatrix} \begin{pmatrix} x_i \\ \dfrac{\mathrm{d}x_i}{\mathrm{d}t} \end{pmatrix}_0 , \tag{46}$$

where the matrix elements are determined by integrating the equations of motion along the cooling zone, given unity initial conditions. Thus, for the initial conditions $x_i(0) = 1$, $\mathrm{d}x_i(0)/\mathrm{d}t = 0$ upon flight through the cooling zone, we have

$$\begin{pmatrix} A_{11} \\ A_{21} \end{pmatrix} = \begin{pmatrix} x_i(\tau) \\ \dfrac{\mathrm{d}x_i(\tau)}{\mathrm{d}t} \end{pmatrix} , \tag{47}$$

where τ is the flight time through the cooling zone.

An essential feature of matrix (46) is that its determinant is no longer necessarily equal to unity, since the system is not closed. During motion in the accelerator, ions interact at each revolution with new electrons, and the electrons may add energy to the system or extract energy from it. For simplification of the analysis we shall assume arrival in the electron beam and departure from it to be sufficiently rapid.

To present a simple example we shall analyze the determinant of matrix (46) for heavy particles interacting with electrons in the absence of a magnetic field. In this case one can limit the analysis to one-dimensional motion and write the equations

$$\begin{aligned} \frac{\mathrm{d}^2 x_e}{\mathrm{d}t^2} &= \omega_{ei}^2 (x_i - x_e) , \\ \frac{\mathrm{d}^2 x_i}{\mathrm{d}t^2} &= \omega_{ie}^2 (x_e - x_i) . \end{aligned} \tag{48}$$

For the coordinate difference $\Delta x = x_e - x_i$ the equation has a simple form

$$\frac{\mathrm{d}^2 \Delta x}{\mathrm{d}t^2} + (\omega_{ei}^2 + \omega_{ie}^2)\Delta x = 0 . \tag{49}$$

As a result, matrix (46) can be represented as follows

$$A = \begin{pmatrix} \dfrac{\omega_{ei}^2 + \omega_{ie}^2 \cos(\omega\tau)}{\omega^2} & \dfrac{\tau\omega_{ei}^2}{\omega^2} + \dfrac{\omega_{ie}^2 \sin(\omega\tau)}{\omega^3} \\ -\dfrac{\omega_{ie}^2 \sin(\omega\tau)}{\omega} & \dfrac{\omega_{ei}^2 + \omega_{ie}^2 \cos(\omega\tau)}{\omega^2} \end{pmatrix} , \tag{50}$$

where $\omega = \sqrt{\omega_{ei}^2 + \omega_{ie}^2}$ is the frequency of oscillations of the beam centers relative to each other.

Figure 18 plots the variation of the determinant of matrix A with the rise of ion density written as $\omega\tau$. It is seen that in the case of a low ion density the response of electrons is positive: ions transfer their energy of transverse motion to electrons, and this is the region of rapid attenuation of coherent oscillations. However, if the ion densities are high, situations arise when after disruption of bonds between the ions and electrons the energy in the ion beam becomes larger than at the beginning! Interaction in the initial zone corresponds to the rapid cooling of coherent oscillations, but if the density of the ion beam is too high, self-heating of coherent fluctuations arises.

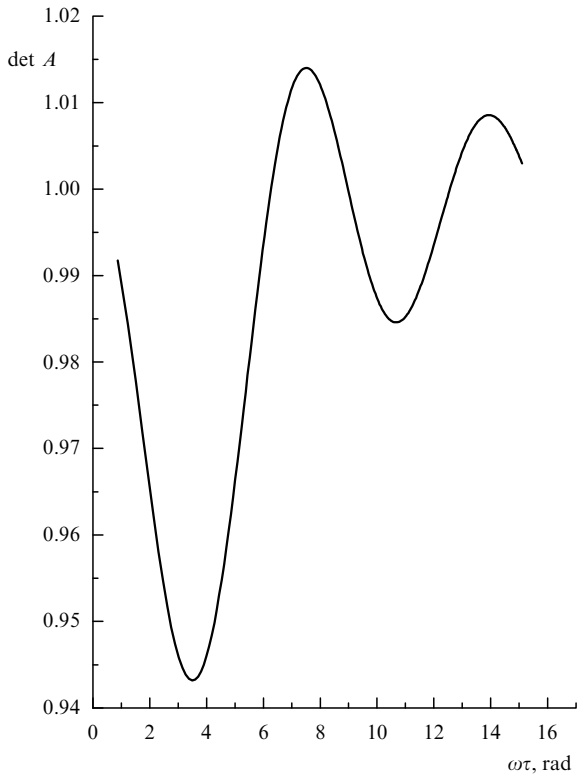

Figure 18. Variation of the determinant of matrix A with an increase of the ion density ($n_e = 10^8$ cm^{-3}, $n_i^{max} = 10^8$ cm^{-3}, $\tau = 4 \times 10^{-8}$ s).

Outside the cooling zone the motion of the ion beam is considered linear and is described by the Twiss matrix

$$\begin{pmatrix} \cos\mu_x & \dfrac{\beta_x}{V_0}\sin\mu_x \\ -\dfrac{V_0}{\beta_x}\sin\mu_x & \cos\mu_x \end{pmatrix} \tag{51}$$

with account taken of reduction of the coordinate from the center to the beginning of the cooling zone in accordance with the relation

$$x = x - V_x \frac{\tau}{2} . \tag{52}$$

After passage through the cooling zone this operation is repeated, before application of the Twiss matrix, for formal reduction of the particle to the center of the cooling zone.

Joint application of the storage ring matrix and the matrix A obtained by numerical integration of the equations of motion and tracing a large number of revolutions in the storage ring permits the stability conditions of oscillations to be obtained for concrete parameters of the storage ring. Figure 19 shows the stability diagram for ion oscillations in the absence of a magnetic field. The proton velocity amounted to $V_0 = 10^{10}$ cm/s, the length of the cooling zone $l = 4$ m, the values of the beta function $\beta_x = \beta_y = 13$ m. In the figure, the density plane of the ion and electron beams is shown. The region in which the instability increment exceeds the Landau damping constant 10^{-3} is shaded. The solid line indicates the boundary of this region for a Landau damping constant equal to 10^{-4}.

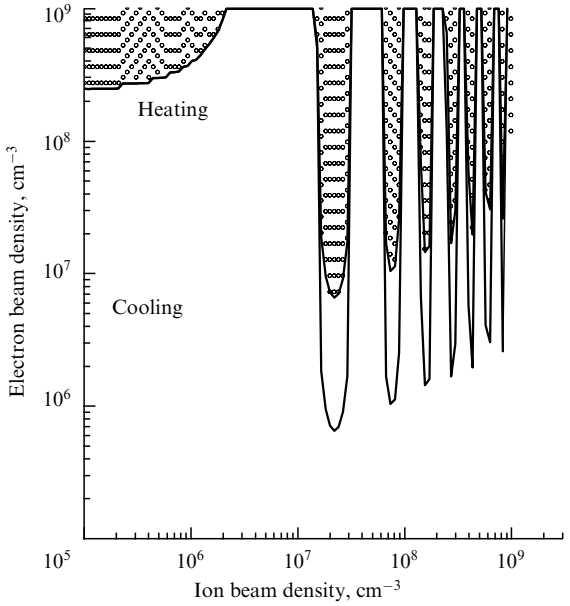

Figure 19. Stability diagram of ion oscillations for $B = 0$ ($\tau = 4 \times 10^{-8}$ s, $l = 4$ m, $\beta_x = 13$ m).

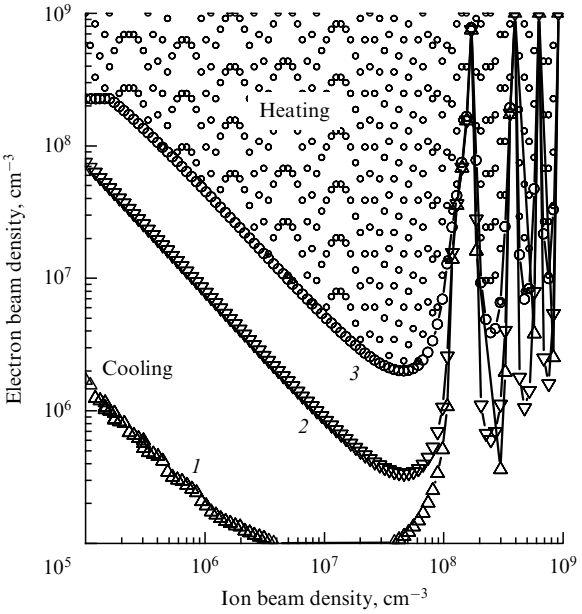

Figure 20. Stability diagram of ion oscillations for $B = 100$ G ($\tau = 4 \times 10^{-8}$ s, $l = 4$ m, $\beta_x = 13$ m).

From Fig. 19 it is seen that in the case of low ion beam densities the restrictions on the electron beam density are related to the excessively large frequency shift of betatron oscillations under the influence of the field of the electron beam space charge. As the ion beam density increases, the electron beam starts oscillating around the ion beam and the restrictions on the dipole modes are even reduced since the action on the ion beam decreases when the electron beam has time to shift toward the center of the ion beam during its flight. Further enhancement of the ion beam density is accompanied by the appearance of instability zones during the unfavorable breakup phase of electron oscillations in the ion beam field.

Introduction of the magnetic field significantly alters the picture of instability zones. Figures 20 and 21 present calculated results taking into account the longitudinal magnetic field applied within the cooling zone with intensities $B = 100$ G and $B = 500$ G, respectively. The region where the instability increment exceeds the Landau damping constant 10^{-3} is shaded. Curve *3* shows the boundary of this zone, curve *2* the boundary of the zone with a damping constant of 10^{-4}, curve *1* the boundary of the zone where coherent interaction gives rise to the damping of coherent oscillations.

From Figs 20 and 21 it is seen that under the condition $n_i n_e \approx 5 \times 10^{13}$ cm^{-6}, the presence of a magnetic field leads to the appearance of a broad instability zone, within which the instability increment approaches the value 10^{-3}, and an increase in the magnetic field weakly influences the location of its boundary. The zone of coherent damping in the line $n_i n_e = 10^{11}$ cm^{-6} corresponds to the parameter $\lambda = \omega_{ei}^2 \omega_{ie}^2 \tau^4 = 1.0 \times 10^{-3}$. Here, the phase incursion of electron oscillations in the coherent beam fields, $\Delta\varphi \approx \sqrt{\lambda M_i/m}$ [see Eqns (42), (43)], approaches unity, while in coherent ion oscillations small (of the order of 10^{-5}) increments arise, which can be suppressed both by Landau damping and by feedback systems. When the value $\lambda \approx 0.1$ is approached, the existence of increments of the order of 10^{-3} makes it more difficult to provide for stability, and when $\lambda \approx 1$ it makes the stability problem practically insoluble.

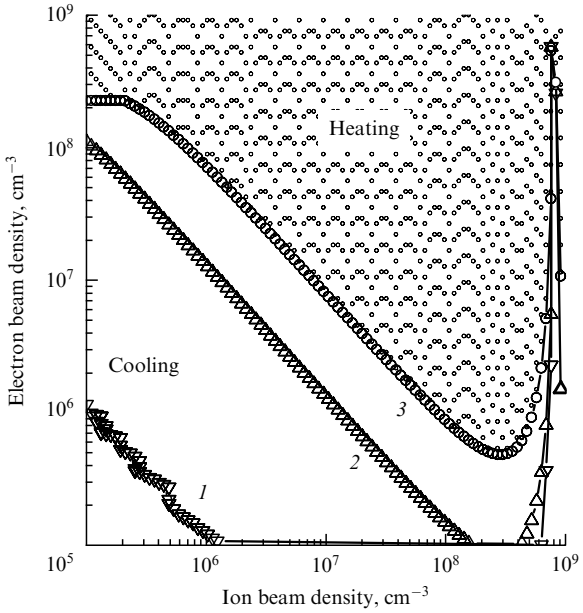

Figure 21. Stability diagram of ion oscillations for $B = 500$ G ($\tau = 4 \times 10^{-8}$ s, $l = 4$ m, $\beta_x = 13$ m).

5. Examples of the application of electron cooling

5.1 Storage of ion beams

In 1998, an electron cooling facility designed and developed at the Nuclear Physics Institute of the RAS Siberian Branch was put into operation [24] at the SIS heavy ion synchrotron in Darmstadt (GSI). After acceleration of the ion beam in the linear accelerator up to an energy of 11 MeV/nucleon and the subsequent stripping of the electrons in a charge exchange target, the ions are made with the aid of multiturn injection to fill up the entire admissible acceptance of the SIS synchrotron (determined by the maximum amplitude of oscillations in the vacuum chamber).

For many kinds of ions it is difficult to obtain a large ion current in the ion source and the linear accelerator, which limits the intensity of the beam accelerated. Electron cooling, which enables the ion beam to be compressed down to a small size, permits multiple injection into the phase volume freed after cooling and thus enhances the accumulated ion beam intensity.

A general view of the electron cooling facility at the SIS synchrotron is presented in Fig. 22. Figure 23 shows an example of the accumulation of bismuth $^{209}Bi^{67+}$ ions in the synchrotron. The parameters of the facility are given in Table 1. From Fig. 23, the losses of ions between injection cycles are seen to rise with the accumulation of ions, and the maximum intensity is achieved when the current losses between injections become equal to the newly injected current. Ion charge exchange on the residual gas and the electron-beam recombination dominate in causing losses. In experiments [24], strong variations of the recombination coefficient were observed, depending on the residual charge of bismuth $^{209}Bi^{(62-68)+}$ ions, similar to the variations observed earlier for lead ions [25, 26].

The radiative recombination coefficient (in units of cm^3/s) of an ion with charge Ze without taking account of the inner electron shell is given by

$$\alpha_{\rm rec} = 3.02 \times 10^{-13} \frac{Z^2}{\sqrt{T_{\rm e}}} \left[\ln \frac{11.32Z}{\sqrt{T_{\rm e}}} + 0.14 \left(\frac{T_{\rm e}}{Z^2} \right)^{1/3} \right], \quad (53)$$

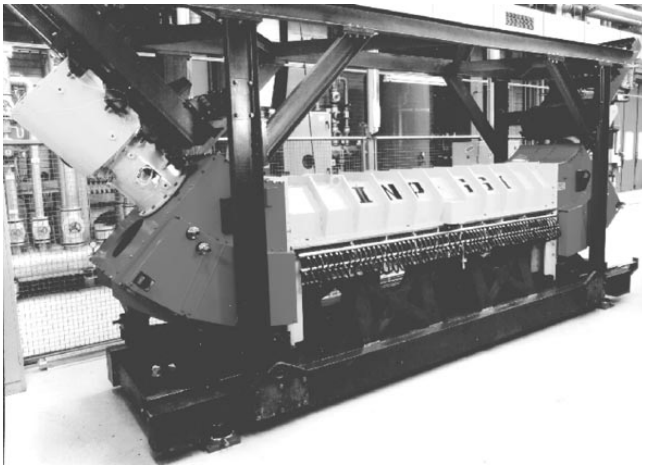

Figure 22. The magnetic system of the electron cooling facility at the SIS synchrotron.

Table 1. Parameters of the electron cooling facility at the SIS synchrotron.

Parameter	Value
Electron beam energy	6.3 keV
Electron beam current	0.3 – 1 A
Cathode diameter	25 mm
Magnetic field at cathode	0.5 – 4 kG
Magnetic field in cooling zone	0.5 – 1.5 kG
Magnetic expansion coefficient	1 – 8
Electron beam diameter	25 – 70 mm
Length of cooling zone	3 m
Parallelism of field in solenoid	5×10^{-5}
Pressure within facility	4×10^{-11} mm Hg

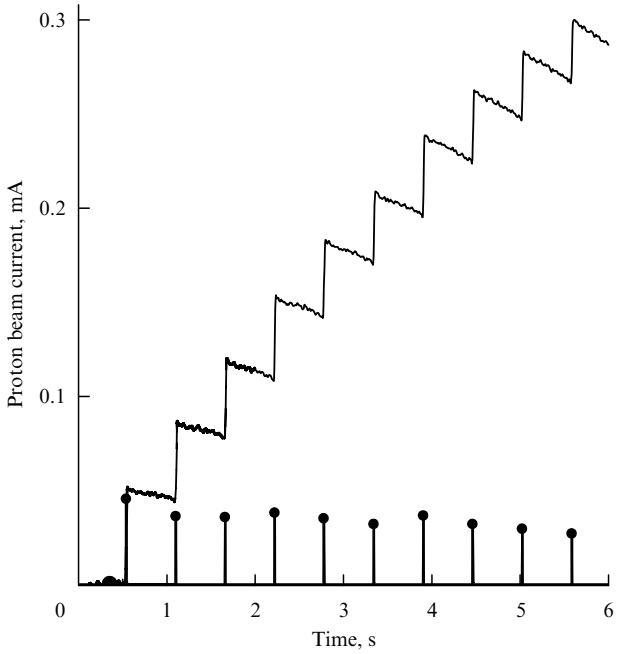

Figure 23. Accumulation of $^{209}Bi^{67+}$ ions at the SIS synchrotron: line — current measured, points — ion current added at each new injection. The cooling electron current $I_{\rm e} = 400$ mA, the expansion factor of the electron beam is 3.

where $T_{\rm e}$ is the electron beam temperature in electron-volts. In the measurements presented in Fig. 24, cooling was performed at the same time as expansion of the ion beam, which reduced its density by a factor of three and, correspondingly, the beam temperature fell from 0.09 to 0.03 eV. The recombination rate for certain partially ionized ions is seen to be close to this estimate.

Studies carried out at the TSR facility revealed that the rapid recombination of certain ions is caused by dielectronic radiationless recombination, when an electron of the beam is captured by an ion and its energy is transferred to an inner electron that undergoes transition to an excited state [26]. If the spectrum of such an interaction has a maximum close to the low energy of relative motion, this leads to the enhanced recombination of such ions.

The most simple way to overcome recombination drawback is to enhance the transverse electron beam temperature, which weakly influences the cooling time in a strong magnetic field but directly affects the rate of recombination. The cooling time of an ion beam with a transverse velocity $V_\perp = \gamma\beta c\sqrt{\epsilon/\beta_\perp}$ (here, ϵ is the ion beam emittance) is defined by the expression

$$\tau^{-1} = c \frac{2n_{\rm e} r_{\rm e} r_{\rm i} L_{\rm c}}{(V_\perp/c)^3}. \quad (54)$$

Taking into account only radiative recombination we obtain an estimate of the ion current accumulation factor in the form

$$N_{\rm storage} = \frac{1}{\alpha_{\rm rec} n_{\rm e} \tau} = \sqrt{T_{\rm e}} \, \frac{8.4 \times 10^{-6}}{A(V_\perp/c)^3}. \quad (55)$$

In the conditions of the experiment for accumulating $^{209}Bi^{67+}$ ions at SIS ($T_{\rm e} = 0.03$ eV, the radial emittance $\epsilon = 150\pi$ mm mrad), the accumulation factor $N_{\rm storage} = 20$, which

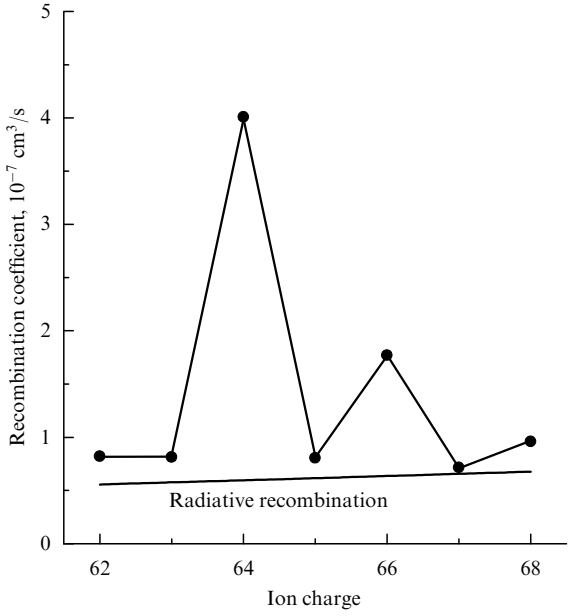

Figure 24. Recombination coefficient of bismuth $^{209}Bi^{(62-68)+}$ ions. The line of radiative recombination is drawn in accordance with Ref. [24] for the effective electron temperature $T_e = 0.03$ eV.

is close to the values obtained in the course of experiments. From expression (55) it is seen that for a substantial enhancement in the accumulation factor it is possible to apply two-stage procedures, in which the ion beam is compressed in one electron beam and, when the beam size (and, subsequently, the transverse velocity $V_\perp$) is essentially reduced, it is retained within another electron beam with a significantly lower density. Here, a reduction of the transverse velocity $V_\perp$ by one order of magnitude should improve the accumulation factor N_{storage} by three orders of magnitude.

Such manipulations are feasible even in a single storage ring, but require a special electron distribution — with a sharply reduced density at the center of the electron beam. This is particularly important, for instance, for the project of a heavy ion collider under development at CERN, which may require for the accumulation of totally ionized lead ions the development of schemes involving reduced ion recombination and a special distribution of the electron beam.

5.2 Experiments with cooled ion beams

The possibility of accumulating beams of partially or totally ionized ions in storage rings and retaining them for many hours has enabled a series of previously inaccessible experiments to be performed. For example, the beta decay of totally ionized dysprosium ions ($A = 163$, $Z = 66$), which are stable in their usual state, was investigated at the ESR electron cooling facility of GSI. In the case of certain nuclei, ionization opens the possibility of beta decay involving the capture of the produced electron to deep-lying atomic levels, thus reducing the energy required for the decay. Such processes take place inside stars where ions are strongly ionized, so the possibility of laboratory investigation of these processes helps achieve a more profound understanding of nucleosynthesis in the Universe and of the abundance of isotopes in stars [27]. An energy of translational ion motion amounting to hundreds of MeV/nucleon permits ions to be ionized by stripping them on a target (nearly like in the depths of stars), while electron cooling down to superlow temperatures allows these ions to be retained in a storage ring for many hours for their properties to be investigated.

Study of the interaction of ions possessing a part of their atomic electrons with cold electrons or with monochromatic laser photons enables interesting information to be obtained with a resolution exceeding 10^{-6} eV. As already mentioned, experiments revealed a strong dielectronic recombination of ions involving one beam electron and another, orbital, electron. Experiments involving complex multiply charged ions are performed at some facilities [28].

A cooled ion beam exhibits a very small momentum spread, which permits very precise measurements of the energies and masses of ions, including long-lived ions with metastable nuclei. Measurement of the beam noise spectrum of short-lived ions involves an uncertainty in the determination of the center of the line created by the ions amounting to $\Delta p/p = \xi T_0/\tau_{\text{life}}$, where ξ is the measurement error depending on noises and the accumulated statistic, τ_{life} is the ion lifetime, T_0 is the revolution time, and T_0/τ_{life} is the natural linewidth. The measurement accuracy of relative particle momenta achieved at the ESR facility [27] is 10^{-7}, which permits precision spectroscopy of a beam of heavy ions to be performed.

5.3 Superthin internal target

With the suppression of scattering by the target electron, electron cooling allows a significant increase in the luminosity of facilities with internal targets [10]. The luminosity of such facilities is determined by the effective thickness of the target, n_t, and the accumulated current ef_0N:

$$L = f_0 N n_t \,. \tag{56}$$

The accumulated current is determined by the balance between the ions arriving from the source, dN_0/dt, and the losses of ions (reactions with a total cross section σ_0) in the storage ring:

$$\frac{dN}{dt} = -\sigma_0 L + \frac{dN_0}{dt} \,. \tag{57}$$

The choice of a superthin target is dictated by the possibility of achieving by cooling the maximum luminosity of the facility, $L = \sigma_0^{-1}\, dN_0/dt$, when all the incoming particles are lost via the channel characterized by the loss cross section σ_0. However, as the amount of incoming ions rises, the number of particles confined in the storage ring also increases, and problems may arise with the beam stability.

The main process causing ion losses from the beam at relatively low energies is a Coulomb scattering by the target nuclei. The scattering cross section is given by

$$\sigma_0 = \frac{4\pi r_p^2 Z^2 Z_t^2}{\gamma^2 \beta^4 A^2 \Delta\theta^2} \,, \tag{58}$$

where Z_t is the charge of the target nuclei, and $\Delta\theta$ is the maximum scattering angle from the target admissible by the aperture of the storage ring. If the target density per unit area is n_t, the probability of scattering at an angle exceeding the aperture angle $\Delta\theta$ equals $\sigma_0 n_t$, and the lifetime of the beam is

$$\tau_{\text{life}} = \frac{1}{f_0 \sigma_0 n_t} \,. \tag{59}$$

To be concrete, we shall illustrate electron cooling using the example of a liquid-hydrogen droplet target at the

CELSIUS facility. Such a target has the important feature that the effective target density is a function of the ion beam dimensions. The target represents a flux of liquid-hydrogen droplets of density $\rho = n_{\rm H} M$, radius $a_{\rm d} = 25$ μm and with distances $\Delta s = 1$ mm between them. Since the size of the target is less than the size of the proton beam, compression by electron cooling enhances the effective target density $n_{\rm t0}$ for the beam.

The geometrical thickness of the target in a beam of radius a (the ion beam Gaussian profile) is equal to

$$n_{\rm t0} = n_{\rm H} \frac{2\sqrt{\pi} a_{\rm d}^3}{3a\Delta s}\,, \tag{60}$$

which for the target parameters of CELSIUS and a beam of radius $a = 4$ mm yields an effective target density $n_{\rm t0} = 3.7 \times 10^{16}\ {\rm cm}^{-2}$.

Figure 25 plots the change in the proton beam current versus time with and without electron cooling. The 48-MeV beam is injected and, then, accelerated up to 400 MeV, which is accompanied by a kinematic enhancement of the proton current owing to the increase in velocity. At the instant of time 30 s the target is switched on and cooling starts. The lower part of the figure shows the rate, normalized to the beam current, with which the products of the proton beam reaction with the target are registered by the WASA detector.

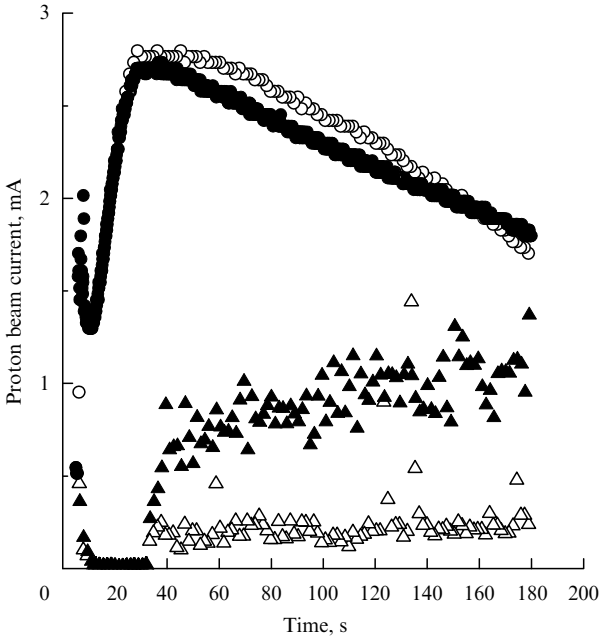

Figure 25. Time variation of proton beam current for interaction with CELSIUS droplet target and of the luminosity normalized to proton current in the case of electron cooling (full points) and without electron cooling (empty points).

From Fig. 25 in the absence of cooling the beam can be seen to expand up to the walls of the vacuum chamber and to rapidly die out, the lifetime of the beam falling to 160 s. When electron cooling takes place, only single-stage processes remain, and the proton beam current decreases exponentially with time in the neighborhood of 330 s. Usually electron cooling enhances the lifetime much more strongly, but in this case the compression of the proton beam also intensifies single scattering by the thin target, which partly compensates for the suppression of multiple scattering.

The luminosity normalized to the beam current remains practically constant during the decay of the proton beam current, thus demonstrating the size of the beam to be constant. The luminosity is five – seven times larger in the case of electron cooling than without cooling. This indicates that the radius of the proton beam undergoes contraction during cooling from 20 – 25 down to 4 mm.

The aperture restrictions imposed on the beam radius amount to approximately 3 cm, while the maximum scattering angle $\Delta\theta = 4 \times 10^{-3}$ rad. Estimating the effective thickness of the target from the lifetime of the cooled beam (equal to 330 s), we find from Eqns (59), (58) $n_{\rm t} = 3.16 \times 10^{16}\ {\rm cm}^{-2}$, which is in reasonable agreement with the geometrical thickness of the target. In the case of 20-mA proton beam, the luminosity of such a facility can reach $5 \times 10^{33}\ {\rm cm}^{-2}\ {\rm s}^{-1}$.

The equilibrium between heating by scattering from the target and cooling is governed by the equation

$$\frac{{\rm d}\theta^2}{{\rm d}t} = -\frac{2n_{\rm e} Z^2 r_{\rm e} r_{\rm p} c L_{\rm c} l_{\rm c}}{A^2\gamma^5\beta^3\pi R} \frac{\theta^2}{(\theta^2+\theta_{\rm e}^2)^{3/2}} + \frac{4\sqrt{\pi} Z^2 Z_{\rm t}^2 r_{\rm p}^2 c L_{\rm t}}{3A^2\gamma^2\beta^3 R} \frac{n_{\rm H} a_{\rm d}^3}{\beta_\perp \theta \Delta s}\,, \tag{61}$$

and the equilibrium angles by the equation

$$\frac{\theta^3}{(\theta^2+\theta_{\rm e}^2)^{3/2}} = \frac{2\pi^{3/2}\gamma^3 Z_{\rm t}^2 m L_{\rm t}}{3ML_{\rm c}} \frac{n_{\rm H} a_{\rm d}^3}{n_{\rm e} l_{\rm c} \beta_\perp \Delta s}\,. \tag{62}$$

A characteristic feature of equation (62) is the absence of an equilibrium value for an excessively large target thickness, when the right-hand side becomes larger than unity:

$$n_{\rm thresh} = \frac{n_{\rm H} a_{\rm d}^3}{\beta_\perp \Delta s} > n_{\rm e} l_{\rm c} \frac{3ML_{\rm c}}{2\pi^{3/2}\gamma^3 Z_{\rm t}^2 m L_{\rm t}}\,. \tag{63}$$

A second salient feature of equation (62) is that in the case of low target densities the important role of the effective electron angles $\theta_{\rm e}$ becomes evident, since the established values of θ depend strongly on them: $\theta \approx \theta_{\rm e}(n_{\rm t0}/n_{\rm thresh})^{1/3}$. As a result, the quality of the magnetic fields in the cooler determines, to a significant degree, the luminosity of the facility. Reduction of $\theta_{\rm e}$ leads to a proportional decrease in the established angular spreads in the ion beam, which is practically always important when performing experiments.

5.4 New projects involving electron cooling

New complexes for heavy-ion studies are under construction in Japan (RIKEN, project MUSES) [29] and P.R. China (IMP, project CSR) [30]. At these centers, several storage rings with electron cooling are to be created. To start with, the primary ion beam from the injector, accumulated in one of the rings, will be dumped onto the target, providing for the production of short-lived nuclei far from the line of stability. Then the nuclei produced will be captured into the second storage ring, and after electron cooling they will be utilized for studies as targets or for further experiments as a beam. The creation of an electron storage ring planned in the project MUSES will permit investigation of the structure of unique nuclei leaving the target and having a lifetime of at least several seconds, sufficient for cooling and achieving the necessary luminosity in electron – ion collisions.

The FNAL project aimed at using electron cooling for secondary cooling of antiprotons (after the duty cycle) will

permit a noticeable increase in the luminosity of the proton–antiproton collider. For this purpose, an electron current of the order of 1 A and energy 5 MeV is to be used [31]. Experiments, recently completed at FNAL, on the recuperation of a 0.7-A electron current in the electrostatic accelerator PELETRON at 1.5 MeV showed that it was possible to achieve the necessary parameters of the electron beam.

Projects involving electron cooling at higher energies (up to the maximum beam energies in the Tevatron and at HERA — about 1 TeV) are under discussion, and theoretical papers in this field are published regularly [32]. However, decisions to make large investments for realization of these projects have yet to be adopted.

5.5 Ion colliders with continuous electron cooling

The new generation of electron–positron colliders (B- and ϕ-factories) that have started operating successfully at many accelerator centers has led to renewed interest in attempts to develop something similar for ion colliders with strong continuous cooling of the ion beam. Strong cooling permits accumulation of intense beams of rare ions and suppression of the destruction of the ion beam due to scattering processes both inside bunches and on the colliding beam [33]. The colliding beams may be very diverse: ion, electron, positron with different energies and polarizations.

We shall make use of the example of a symmetric ion collider to show how electron cooling aids in enhancing the luminosity of the facility. The luminosity of an ion collider depends on the beam parameters:

$$L = \frac{N}{4\pi\sigma_\perp^2}\,\frac{NV_0}{D_\mathrm{b}}\,, \tag{64}$$

where $\sigma_\perp$ is the transverse size of bunches at the collision site, N is the number of particles in a bunch, V_0 is the velocity of motion of a bunch, and D_b is the distance between bunches.

Cooling reduces the beam emittance and permits the luminosity to be enhanced at the expense of a decrease in $\sigma_\perp$ and an increase in N by accumulation of new portions of particles. In so doing, the cooling and accumulation cycles can be realized not only at the total beam energy, but wherever it is most convenient. However, so-called beam–beam effects in collisions when beams are too intense cause a rapid rise in the beam emittances.

The strength of this interaction is characterized by the space charge parameter

$$\xi = \frac{Nr_\mathrm{i}}{4\pi\epsilon_\mathrm{n}}\,, \tag{65}$$

where $\epsilon_\mathrm{n} = \gamma\beta\sigma_\perp^2/\beta^*$ is the normalized beam emittance, β^* is the value of the beta function at the collision site. The luminosity can, then, be written as

$$L = \xi\,\frac{\gamma\beta}{r_\mathrm{i}\beta^*}\,\frac{Nv}{D_\mathrm{b}}\,. \tag{66}$$

For obtaining the limit luminosities, strong focusing, which reduces β^*, is required at the collision site, as well as short intense bunches (shorter than β^*). For example, in electron–positron colliders yielding an energy of 5 GeV it turns out to be possible for $\gamma = 10^4$, $\beta^* = 2$ cm to obtain the value $\xi \approx 0.05$, and for medium beam currents of 1 A ($NV_0/D_\mathrm{b} = 6\times10^{18}\ \mathrm{s}^{-1}$) the luminosity $L = 5\times10^{33}\ \mathrm{cm}^{-2}\,\mathrm{s}^{-1}$. Experience shows that without cooling it is quite difficult even to achieve the value $\xi \approx 0.005$. Strong cooling signifies that during the cooling time the beam makes approximately 3×10^6 revolutions.

For understanding the scale of the phenomenon, the main parameters of a uranium–uranium collider yielding beams with an energy of 15 GeV/nucleon are presented in Table 2. The data on the limiting luminosity value depend on the optimism in obtaining a large ξ value.

Table 2. Parameters of a uranium–uranium collider with electron cooling.

Parameter	Value
Electron beam energy	30 MeV
Impulse current of electron bunch	0.3 A
Average current	4 mA
Length of cooling zone	13 m
Number of particles	3×10^8
Length of ion bunch	10 cm
Normalized beam emittance	0.3–0.03 mm mrad
Space charge parameter ξ	0.005–0.05
Luminosity	10^{28}–$10^{29}\ \mathrm{cm}^{-2}\,\mathrm{s}^{-1}$

In principle, facilities with the electron beams necessary for such cooling are created within the framework of activities in the development of free electron lasers [34]. However, electron cooling is very sensitive to the dispersion of transverse electron velocities in the cooling zone. Utilization of a strong magnetic field, as already discussed, aids in enhancing the cooling but, as a rule, it is difficult to provide for the presence of the magnetic field along the entire acceleration path. The development of optical schemes for high-voltage cooling with a longitudinal magnetic field only in the region of the electron source and along the cooling zone is a task that has still to be investigated.

The most interesting scientific problem for colliders with electron cooling is finding a way of overcoming instability in the system comprising the ion beam and the cooling electrons. The space charge parameter of an ion bunch (the square of the phase shift of electron oscillations in the field of the ion bunch) acting on the electrons is many times larger than the ion–ion interaction:

$$\xi_\mathrm{ei} = (\omega_\mathrm{ei}\tau)^2 = \frac{Nr_\mathrm{e}l_\mathrm{cool}^2}{\epsilon_\mathrm{n}\gamma^2\beta^2} = \xi\,\frac{4\pi l_\mathrm{cool}^2}{\beta_\mathrm{cool}\beta^*(\gamma\beta)^2}\,\frac{MA_\mathrm{i}}{mZ_\mathrm{i}}\,. \tag{67}$$

For the collider parameters given in Table 2, the amplification factor amounts to $\xi_\mathrm{ei} = 2.5\times10^4\xi$, which corresponds to $\xi_\mathrm{ei} = 12-125$ for $\xi = 0.001-0.01$. Experiments reveal that problems arise, when $\xi_\mathrm{ei} \approx 1$. The creation of several cooling zones together with a corresponding reduction in the length of each zone may turn out to be essential for resolving these problems. However, the stability of systems with a larger number of cooling zones requires additional studies.

6. Conclusions

Electron cooling today is a rapidly developing field of accelerator science and technology. Many facilities have been created since the middle of the 60s, when G I Budker put forward this idea. The facilities with electron cooling under construction in Japan and P.R. China will doubtless broaden the possibilities of experiments with unique nuclei. The project for the development of electron cooling for the

American antiproton complex at FNAL will extend the high-voltage limit up to electron energies of 5 MeV.

In conclusion, the authors wish to thank those colleagues who participated from the very beginning in the development of electron cooling: Ya S Derbenev, N S Dikanskiĭ, V I Kononov, V I Kudelaĭnen, I N Meshkov, D V Pestrikov, R A Salimov, and B N Sukhina for their creative contribution to this field of science and acceleration technology. The efforts of the staff of the Nuclear Physics Institute of the RAS Siberian Branch in the development of electron cooling has opened to the world scientific community one more instrument for perceiving nature.

The authors express gratitude to Dag Reistad (TSL, Uppsala) for the possibility of participating in experiments at CELSIUS and stimulating discussions, M Steck (GSI, Darmstadt) and D Möhl (CERN) for useful and interesting discussions of the problems of electron cooling.

References

1. Kolomenskiĭ A A, Lebedev A N *Teoriya Tsiklicheskikh Uskoriteleĭ* (Theory of Cyclic Accelerators) (Moscow: Fizmatgiz, 1962) [Translated into English (Amsterdam: North-Holland, 1966)]
2. Budker G I *Atomnaya Energiya* **22** 346 (1967)
3. Derbenev Ya S, Skrinsky A N *Particle Acceleration* **8** 1 (1977)
4. Kudelaĭnen V I, Meshkov I N, Salimov R A *Zh. Tekh. Fiz.* **41** 2294 (1971)
5. Kudelaĭnen V I et al. *Zh. Tekh. Fiz.* **46** 1678 (1976) [*Sov. Phys. Tech. Phys.* **21** 965 (1976)]
6. Budker G I et al. *IEEE Trans. Nucl. Sci.* **NS-22** 2093 (1975)
7. Budker G I et al., in *Trudy 5-go Vsesoyuznogo Soveshchaniya po Uskoritelyam Zaryazhennykh Chastits* (Proceedings of the 5th All-Union Symposium on Charged Particle Accelerators) (Dubna, 1976) Vol. 1 (Moscow: Nauka, 1977) p. 236
8. Budker G I et al. *Particle Acceleration* **7** 197 (1976)
9. Derbenev Ya S, Skrinsky A N *Fiz. Plazmy* **4** 492 (1978) [*Sov. J. Plasma Phys.* **4** 273 (1978)]; *Sov. Sci. Rev. Sec. A Phys. Rev.* 165 (1981)
10. Budker G I, Skrinskiĭ A N *Usp. Fiz. Nauk* **124** 561 (1978) [*Sov. Phys. Usp.* **21** 277 (1978)]
11. Dikanskiĭ N S et al., Preprint of the Nuclear Physics Institute, USSR AS Siberian Branch (Novosibirsk: IYaF SO AN SSSR, 1987) pp. 87
12. Parkhomchuk V V, Skrinsky A N *Rep. Prog. Phys.* **54** 921 (1991)
13. Parkhomchuk V V, Pestrikov D V *Zh. Tekh. Fiz.* **50** 1411 (1980) [*Sov. Phys. Tech. Phys.* **25** 818 (1980)]
14. Steck M et al. *Phys. Rev. Lett.* **77** 3803 (1996)
15. Wei J et al., in *Proc. 31st Workshop of INFN Eloisatron Project* (Erice, Italy, 12 – 21 Nov. 1995) (Erice: World Scientific, 1995)
16. Schramm U et al., in *Workshop Electron Cooling 99* (Uppsala, Sweden, 1999); *Nucl. Instrum. Methods Phys. Res. A* **441** 209 (2000)
17. Reistad D et al., in *Proc. Workshop on Beam Cooling and Related Topics* (Montreux, Switzerland, 4 – 8 Oct. 1993) [CERN (Series), 94-03, Ed. J Bosser] (Geneva: European Organization for Nuclear Research, 1994) p. 183
18. Anderson D et al., in *Proc. Workshop on Beam Cooling and Related Topics* (Montreux, Switzerland, 4 – 8 Oct. 1993) [CERN (Series), 94-03, Ed. J Bosser] (Geneva: European Organization for Nuclear Research, 1994) p. 377
19. Stein J et al., in *Medium Energy Electron Cooling Workshop* (Dubna, Russia, 15 Sept. 1998)
20. Bosser J et al., in *Workshop Electron Cooling 99* (Uppsala, Sweden, 1999); *Nucl. Instrum. Methods Phys. Res. A* **441** 1 (2000)
21. Dikanskiĭ N S, Pestrikov D V *Fizika Intensivnykh Puchkov v Nakopitelyakh* (The Physics of Intense Beams in Storage Rings) (Novosibirsk: Nauka, 1989) [Translated into English (New York: AIP, 1994)]
22. Parkhomchuk V V, Pestrikov D V, in *Proc. Workshop on Beam Cooling and Related Topics* (Montreux, Switzerland 4 – 8 Oct. 1993) [CERN (Series), 94-03, Ed. J Bosser] (Geneva: European Organization for Nuclear Research, 1994) p. 327
23. Parkhomchuk V V, in *Recent Development in Electron Cooling and Its Applications* APAC'98 (Tsukuba, Japan, 1998) p. 462
24. Steck M et al., in *Proc. 6th EPAC'98* (Stockholm, 1998)
25. Baird S et al. *Phys. Lett. B* **361** 184 (1995)
26. Wolf A et al., in *Workshop Electron Cooling 99* (Uppsala, Sweden, 1999); *Nucl. Instrum. Methods Phys. Res. A* **441** 183 (2000)
27. "Highlights from three years of SIS/ESR operation at GSI" *Nuclear Physics News* **3** 14 (1993)
28. "Cooler Ring TARN-2" *Nuclear Physics News* **8** 31 (1998)
29. Tanabe T et al. *Nucl. Instrum. Methods Phys. Res. A* **441** 104 (2000)
30. Rao Y *HIRFL-CSR Design Parameters* (CSR Division, Institute of Modern Physics, P.O. Box 31, Lanzhou, 730000, P.R. China, March 6, 2000)
31. Nagaitsev S et al. *Nucl. Instrum. Methods Phys. Res. A* **441** 241 (2000)
32. Balevski K et al. *Nucl. Instrum. Methods Phys. Res. A* **441** 274 (2000)
33. Skrinsky A N *Nucl. Instrum. Methods Phys. Res. A* **441** 286 (2000)
34. Vinokurov N A et al., in *Second Asian Symp. on Free Electron Laser* (Novosibirsk, Russia, 1995) p. 39